Ground-level gaseous pollutants (NO_2, SO_2, and CO) in China: daily seamless mapping and spatiotemporal variations

Jing Wei[1*], Zhanqing Li[1*], Jun Wang[2], Can Li[1], Pawan Gupta[3,4], Maureen Cribb[1]

1. Department of Atmospheric and Oceanic Science, Earth System Science Interdisciplinary Center, University of Maryland, College Park, MD, USA
2. Department of Chemical and Biochemical Engineering, Iowa Technology Institute, Center for Global and Regional Environmental Research, University of Iowa, USA
3. STI, Universities Space Research Association (USRA), Huntsville, AL, USA
4. NASA Marshall Space Flight Center, Huntsville, AL, USA

* Correspondence: Zhanqing Li (zhanqing@umd.edu); Jing Wei (weijing@umd.edu)

Abstract

Gaseous pollutants at the ground level seriously threaten the urban air quality environment and public health. There are few estimates of gaseous pollutants that are spatially and temporally resolved and continuous across China. This study takes advantage of big data and artificial intelligence technologies to generate seamless daily maps of three major ambient pollutant gases, i.e., NO_2, SO_2, and CO, across China from 2013 to 2020 at a uniform spatial resolution of 10 km. Cross-validation between our estimates and ground observations illustrated a high data quality on a daily basis for surface NO_2, SO_2, and CO concentrations, with mean coefficients of determination (root-mean-square errors) of 0.84 (7.99 $\mu g/m^3$), 0.84 (10.7 $\mu g/m^3$), and 0.80 (0.29 mg/m^3), respectively. We found that the COVID-19 lockdown had sustained impacts on gaseous pollutants, where surface CO recovered to its normal level in China on around the 34^{th} day after the Lunar New Year, while surface SO_2 and NO_2 rebounded more than twice slower due to more CO emissions from increased residents' indoor cooking and atmospheric oxidation capacity. Surface NO_2, SO_2, and CO reached their peak annual concentrations of 21.3 ± 8.8 $\mu g/m^3$, 23.1 ± 13.3 $\mu g/m^3$, and 1.01 ± 0.29 mg/m^3 in 2013, then continuously declined over time by 12%, 55%, and 17%, respectively, until 2020. The declining rates were more prominent from 2013 to 2017 due to the sharper reductions in anthropogenic emissions but have slowed down in recent years. Nevertheless, people still suffer from high-frequency risk exposure to surface NO_2 in eastern China, while surface SO_2 and CO have almost reached the recommended air quality guidelines level since 2018, benefiting from the implemented stricter "ultra-low" emission standards. This reconstructed dataset of surface gaseous pollutants will benefit future (especially short-term) air pollution and environmental health-related studies.

1. Introduction

Air pollution has been a major environmental concern, affecting human health, weather, and climate (Kinney, 2008; Sun et al., 2010; Kan et al., 2012; Z. Li et al., 2017; Murray et al., 2020; Orellano et al., 2020; Anenberg et al., 2022), thus drawing worldwide attention. The sources of air pollution are complex. They include natural sources such as wildfires and anthropogenic emissions, including pollutants discharged from industrial production [e.g., smoke/dust, sulfur oxides, nitrogen oxides (NO_x), and volatile organic compounds (VOCs)], hazardous substances released from burning coal during heating seasons [e.g., dust, sulfur dioxide (SO_2), and carbon monoxide (CO)], and waste gases (e.g., CO, SO_2, and NO_x) generated by transportation, especially in big cities.

Among various air pollutants, the following have been most widely recognized: particulate matter with diameters smaller than 2.5 μm and 10 μm ($PM_{2.5}$ and PM_{10}) and gaseous pollutants [e.g., ozone (O_3), nitrogen dioxide (NO_2), SO_2, and CO, among others]. Many countries have built ground-based networks to monitor a variety of conventional pollutants in real time. China has experienced serious ambient air pollution for a long time, prompting the establishment of a large-scale air quality monitoring network (MEE, 2018a). Over the years, much effort has been made to model different species of air pollutants. Many studies focused on particulate matter in China have been carried out (Fang et al., 2016; T. Li et al., 2017; G. Chen et al., 2018; Z. Zhang et al., 2018; Ma et al., 2022). The global COVID-19 pandemic has motivated many attempts to estimate surface NO_2 concentrations from satellite-retrieved tropospheric NO_2 products (Tian et al., 2020; WHO, 2020), e.g., from the Ozone Monitoring Instrument (OMI) onboard the NASA Aura spacecraft and the TROPOspheric Monitoring Instrument (TROPOMI) onboard the Copernicus Sentinel-5 Precursor satellite, adopting different statistical regression (Qin et al., 2017; Z. Zhang et al., 2018; Chi et al., 2021) and artificial intelligence (Zhan et al., 2018; Z.-Y. Chen et al., 2019; Dou et al., 2021; Liu, 2021; Y. Wang et al., 2021; Chi et al., 2022) models. By comparison, surface SO_2 and CO in China are less studied, limited by weaker signals and a lack of good-quality satellite tropospheric products (D. Liu et al., 2019; R. Li et al., 2020; Y. Wang et al., 2021; W. Han et al., 2022b). Such studies still face more challenges, e.g., satellite data gaps and missing values that seriously limit their application and the neglect of spatiotemporal differences in air pollution in the modeling process. In addition, most previous studies mainly focused on studying a single or a few species during relatively short observational periods.

In view of the above problems, the purpose of this paper is to reconstruct daily concentrations of three ambient gaseous pollutants (i.e., NO_2, SO_2, and CO) in China. To this end, relying on the dense national ground-based observation network and big data, including satellite remote sensing products, meteorological reanalysis, chemical model simulations, and emission inventories, we are capable of mapping three pollutant gases seamlessly (100% spatial coverage) on a daily basis at a uniform spatial resolution of 10 km since 2013 in China. Estimates were made using an extended and powerful machine-learning model incorporating spatiotemporal information, i.e., space-time extra-trees. Natural and anthropogenic effects on air pollution, including their physical mechanisms and chemical reactions, were accounted for in the modeling. Using this dataset, spatiotemporal variations of the gaseous pollutants, the impacts of environmental protection policies and the COVID-19 epidemic, and population risk exposure to gaseous pollution are investigated.

To date, we have combined the advantages of artificial intelligence and big data to construct a virtually complete set of major air quality parameters concerning both particulate and gaseous pollutants over a long period of time across China, including PM_1 (2000–Present, Wei et al., 2019), $PM_{2.5}$ (2000–Present, Wei et al., 2020; Wei et al., 2021a), PM_{10} (2000–Present, Wei et al., 2021b), O_3 (1979–Present, Wei et al., 2022a; He et al., 2022), and NO_2 (2019–Present, Wei et al., 2022b), serving environmental, public health, economy, and other related research. This study is the continuation of our previous studies, which adds two new species of SO_2 and CO for the first time and also dates the data records of NO_2 back to 2013. Instead of devoting itself to a single pollutant, this study deals with all gaseous pollutants of compatible quality over the same period with the same spatial coverage and resolution. In particular, considering that there are few public datasets of these three gaseous pollutants with such spatiotemporal coverages focusing on the whole of China, this is highly valuable for the sake of studying their variations, relative proportions, and attribution of emission sources, as well as their diverse and joint effects of different pollutant species on public health.

2. Materials and methods

2.1 Big data

2.1.1 Ground-based measurements

Hourly measurements of ground-level NO_2, SO_2, and CO concentrations from ~2000 reference-grade ground-based monitoring stations (Figure 1) collected from the China National Environmental Monitoring Centre (CNEMC) network (open-source available at https://www.cnemc.cn/en/) were employed in the study. This network includes urban assessing stations, regional assessing stations, background stations, source impact stations, and traffic stations, set up in a reasonable overall layout that covers industrial (~14%), urban (~31%), suburban (~39%), and rural (~16%) areas to improve the spatial representations, continuity, and comparability of observations (HJ 664-2013) (MEE, 2013a). NO_2 is measured by chemiluminescence and differential optical absorption spectroscopy (DOAS), and SO_2 uses ultraviolet fluorescence and DOAS, while CO adopts non-dispersive infrared spectroscopy and gas filter correlation infrared spectroscopy. These measurements have been fully validated and have the same average error of indication of ±2% F.S. for the three gaseous pollutants considered here, with additional quality-control checks such as zero and span noise and zero and span drift (HJ 193-2013 and HJ 654-2013) (MEE, 2013b, 2013c). They have also been used as ground truth in almost all air pollutant modelling studies in China (Ma et al., 2022; B. Zhang et al., 2022a). All stations use the same technique to measure each gas routinely and continuously 24 hours a day at about the sea level without time series gaps. However, the reference state (i.e., observational conditions like temperature and pressure) changed from the standard condition (i.e., 273 K and 1013 hPa) to the room condition (i.e., 298 K and 1013 hPa) on 31 August 2018 (MEE, 2018a). We thus first converted observations of the three gaseous pollutants after this date to the uniform standard condition for consistency. Here, daily values for each air pollutant were averaged from at least 30% of valid hourly measurements at each station in each year from 2013 to 2020.

[Please insert Figure 1 here]

2.1.2 Main predictors

A new daily tropospheric NO_2 dataset at a horizontal resolution of 0.25° × 0.25° in China (https://doi.org/10.6084/m9.figshare.13126847) was employed, created by Q. He et al. (2020) using a developed framework integrating OMI/Aura Quality Assurance for Essential Climate Variables (QA4ECV) and Global Ozone Monitoring Experiment–2B (GOME-2B) offline tropospheric NO_2 retrievals passing quality controls (i.e., cloud fraction < 0.3, surface albedo < 0.3, and solar zenith angle < 85°). The reconstructed tropospheric NO_2 agreed well (R = 0.75–0.85) with Multi-AXis Differential Optical Absorption Spectroscopy (MAX-DOAS) measurements (H. He et al., 2020). Through this data fusion, the daily spatial coverage of satellite tropospheric NO_2 was significantly improved in China (average = 87%). Areas with a small number of missing values were imputed via a nonparametric machine-learning model by regressing the conversion relationship with Copernicus Atmosphere Monitoring Service (CAMS) tropospheric NO_2 assimilations (0.75° × 0.75°), making sure that the interpolation was consistent with the OMI/Aura overpass time (Inness et al., 2019; Y. Wang et al., 2020). The gap-filled tropospheric NO_2 was reliable compared with measurements (R = 0.94–0.98) (Wei et al., 2022b). The above two-step gap-filling procedures allowed us to generate a daily seamless tropospheric NO_2 dataset that removes the effects of clouds from satellite observations.

Here, the reconstructed daily seamless tropospheric NO_2, together with CAMS daily ground-level NO_2 assimilations (0.75° × 0.75°) averaged from all 3-hourly data in a day and monthly NO_x anthropogenic emissions (0.1° × 0.1°) (Inness et al., 2019), were used as the main predictors for estimating surface NO_2. Limited by the quality of direct satellite observations, daily model-simulated SO_2 and CO surface mass concentrations, averaged from all available data in a day provided by one-hourly Modern-Era Retrospective Analysis for Research and Applications, version 2 (MERRA-2, 0.625° × 0.5°), 3-hourly CAMS (0.75° × 0.75°), and 3-hourly Goddard Earth Observing System Forward-Processing (0.3125° × 0.25°) global reanalyses were used as main predictors to retrieve surface SO_2 and CO, together with CAMS monthly SO_2 and CO anthropogenic emissions.

2.1.3 Auxiliary factors

Meteorological factors have important diverse effects on air pollutants (J. He et al., 2017; R. Li et al., 2019), e.g., the boundary-layer height reflects their vertical distribution and variations (Z. Li et al., 2017; Seo et al., 2017); temperature, humidity, and pressure can affect their photochemical reactions (W. Y. Xu et al., 2011; T. Li et al., 2019; C. Zhang et al., 2019a); and rainfall and wind can also influence their removal, accumulation, and transport (Dickerson et al., 2007; R. Li et al., 2019). Eight daily meteorological variables, provided by the ERA5-Land (0.1° × 0.1°; Muñoz-Sabater et al., 2021) and ERA5 global reanalysis (0.25° × 0.25°; Hersbach et al., 2020), were calculated (i.e., accumulated for precipitation and evaporation while averaged for the others) from all hourly data in a day, used as auxiliary variables to improve the modelling of gaseous pollutants. Other auxiliary remote-sensing data used to describe land-use cover/change [i.e., Moderate Resolution Imaging Spectroradiometer (MODIS) normalized difference vegetation index (NDVI), 0.05° × 0.05°] and population distribution density (i.e., LandScan^{TM}, 1 km) were employed as inputs to the machine-learning model because they are highly related to the type of pollutant emission and amounts of anthropogenic emissions, as well as the surface terrain [i.e., Shuttle Radar Topography Mission (SRTM) digital elevation model (DEM), 90m], which can affect the transmission of air pollutants. Table S1 provides detailed information about all the data used in this study. All variables were aggregated or resampled into a 0.1° × 0.1° resolution for consistency.

2.2 Pollutant gas modelling

Here, the developed Space-Time Extra-Tree (STET) model, integrating spatiotemporal autocorrelations of and differences in air pollutants to the Extremely Randomized Trees (ERT) (Wei et al., 2022a), was extended to estimate surface gaseous pollutants, i.e., NO_2, SO_2, and CO. ERT is an ensemble machine-learning model based on the decision tree, capable of solving the nonparametric multivariable nonlinear regression problem. Ensemble learning can avoid the lack of learning ability of a single learner, greatly improving accuracy. The introduced randomness enhances the model's anti-noise ability and minimizes the sensitivity to outliers and multicollinearity issues. It can handle high latitude, discrete or continuous data without data normalization and is easy to implement and parallel. However, several limitations exist, e.g., it is difficult to make predictions beyond the range of training data, and there will be an over-fitting issue on some regression problems with high noise. The training efficiency diminishes with increasing memory occupation when the number of decision trees is large (Geurts et al., 2006). Compared with traditional tree-based models (e.g., random forest), ERT has a stronger randomness which randomly selects a feature subset at each node split and randomly obtains the optimal branch attributes and thresholds. This helps to create more independent decision trees, further reducing model variance and improving training accuracy (Geurts et al., 2006). The STET model has been successfully applied in estimating high-quality surface O_3 in our previous study (Wei et al., 2022a). It is thus extended here to regress the nonlinear conversion relationships between ground-based measurements and the main predictors and auxiliary factors for other species of gaseous pollutants. For surface NO_2, the STET model was applied to the main variables of the satellite tropospheric NO_2 column, modelled surface NO_2 mass, and NO_x emissions, together with ancillary variables of the previously mentioned meteorological, surface, and population variables (Equation 1). For surface SO_2 (Equation 2) and CO (Equation 3), modelled surface SO_2 and CO concentrations and SO_2 and CO emissions were used as main predictors along with the same auxiliary variables as NO_2 to construct the STET models separately.

$$NO_{2(ijt)} \sim f_{STET}(SNO_{2(ijt)}, MNO_{2(ijt)}, ENOx_{ijm}, Meteorology_{ijt}, NDVI_{ijm}, DEM_{ijy}, POP_{ijy}, P_s, P_t), \quad (1)$$

$$SO_{2(ijt)} \sim f_{STET}(MSO_{2(ijt)}, ESO_{2(ijm)}, Meteorology_{ijt}, NDVI_{ijm}, DEM_{ijy}, POP_{ijy}, P_s, P_t), \quad (2)$$

$$CO_{ijt} \sim f_{STET}\left(MCO_{ijt}, ECO_{ijm}, Meteorology_{ijt}, NDVI_{ijm}, DEM_{ijy}, POP_{ijy}, P_s, P_t\right), \quad (3)$$

where $NO_{2(ijt)}$, $SO_{2(ijt)}$, and CO_{ijt} indicate daily ground-based NO_2, SO_2, and CO measurements at one grid (i, j) on the tth day of a year; $SNO_{2(ijt)}$ indicates the daily satellite tropospheric NO_2 column at one grid (i, j) on the tth day of a year; $MNO_{2(ijt)}$, $MSO_{2(ijt)}$, and MCO_{ijt} indicate daily model-simulated surface NO_2, SO_2, and CO concentrations at one grid (i, j) on the tth day of a year; $ENOx_{ijm}$, $ESO_{2(ijm)}$, and ECO_{ijm} indicate monthly anthropogenic NO_x, SO_2, and CO emissions at one grid (i, j) in the mth month of a year; $Meteorology_{ijt}$ represents each meteorological variable at one grid (i, j) on the tth day of a year; DEM_{ijy} and POP_{ijy} indicate the elevation and population at one grid (i, j) of a year; and P_s and P_t indicate the space and time term (Wei et al., 2022a).

3. Results and discussion

3.1 Seamless mapping of surface gaseous pollutants

Using the constructed STET model, we generated daily 10 km resolution datasets with complete coverage (spatial coverage = 100%) for three ground-level gaseous pollutants from 2013 to 2020 in China, called ChinaHighNO_2, ChinaHighSO_2, and ChinaHighCO. Monthly and annual maps were generated by directly averaging daily data at each grid. They belong to a series of public high-resolution and high-quality datasets of a variety of ground-level air pollutants for China [ChinaHighAirPollutants (CHAP), available at https://weijing-rs.github.io/product.html] developed by our team. Figure 2 shows spatial distributions of the three pollutant gases across China on a typical day (1 January 2018). The spatial patterns of these gaseous pollutants were consistent with those observed on the ground, especially in highly polluted areas, e.g., severe surface NO_2 pollution in the North China Plain (NCP) and high surface SO_2 emissions in Shanxi Province. The unique advantage of our dataset is that it can provide valuable gaseous pollutant information on a daily basis at locations in China where ground measurements are not available. This addresses the major issues of scanning gaps and numerous missing values in satellite remote sensing retrievals at cloudy locations, e.g., the average spatial coverage of the official OMI/Aura daily tropospheric NO_2 product is only 42% over the whole of China during the period 2013–2020 (Figure S1). Our dataset provides spatially complete coverage, significantly increasing daily satellite observations by 58%. In addition, reanalysis data do not simulate surface masses of gaseous pollutants well, underestimating them compared to our results and ground-based observations in China (Figure S2). This is especially so for SO_2, where high-pollution hot spots are easily misidentified. Validation illustrates that our regressed results for surface NO_2, SO_2, and CO agree better with ground measurements than modelled results (slopes are close to 1, and correlations > 0.93), 1.9–6.4 times stronger in slope, 1.3–3.5 times higher in correlation, but 5.9–7.7 times smaller in differences (Figure S3). This shows that our model can take advantage of big data to significantly correct and reconstruct gaseous simulation results via data mining using machine learning.

[Please insert Figure 2 here]

Figure 3 shows annual and seasonal maps for each gas pollutant during the period 2013–2020 across China. Multi-year mean surface NO_2, SO_2, and CO concentrations were 20.3 ± 4.7 μg/m^3, 16.2 ± 7.7 μg/m^3, and 0.86 ± 0.22 mg/m^3, respectively. Pollutant gases varied significantly in space across China, where high surface NO_2 levels were mainly distributed in typical urban agglomerations, e.g., the Beijing-Tianjin-Hebei (BTH) region, the Yangtze River and Pearl River Deltas (YRD and PRD), and scattered large cities with intensive human activities and highly developed transportation systems (e.g., Urumqi, Chengdu, Xi'an, and Wuhan, among others). High surface SO_2 concentrations were mainly observed in northern China (e.g., Shanxi, Hebei, and Shandong Provinces), associated with combustion emissions from anthropogenic sources, and the Yunnan Guizhou Plateau in southwest China, likely associated with emissions from volcanic eruptions. By contrast, except in some areas in central China (e.g., Shanxi and Hebei), surface CO concentrations were overall low.

Significant differences in spatial patterns were seen at the seasonal level. Surface NO_2, SO_2, and CO in summer (average = 15.9 ± 4.7 μg/m^3, 22.9 ± 13.4 μg/m^3, and 1.1 ± 0.3 mg/m^3, respectively) were the lowest, thanks to favorable meteorological conditions, e.g., abundant precipitation and high air humidity conducive to flushing and scavenging of different air pollutants (Yoo et al., 2014). Strong sunlight and high temperature also accelerate the photochemical reactions of NO_2 loss (Shah et al., 2020). Pollution levels were highest in winter, with average values increasing by ~1.5–1.9 times those in summer. This difference was much larger in central and eastern China, e.g., 2.3–3.4 times higher in the BTH due to large amounts of direct NO_x, SO_2, and CO emissions from burning coal for heating in winter in northern China. The spatial patterns of the three gaseous pollutants were similar in spring and autumn.

[Please insert Figure 3 here]

3.2 Changes in gaseous pollution and exposure risk

3.2.1 Short-term epidemic effects on air quality

Many studies have focused on the effects of the COVID-19 epidemic on air quality (WHO, 2020). Most of them were done using ground-based observations (Huang et al., 2020; T. Su et al., 2020), tropospheric gas columns (Field et al., 2021; Levelt et al., 2022), or retrieved surface masses (Ling and Li, 2021; Cooper et al., 2022). The resulting conclusions could be affected by insufficient spatial representation due to the uneven distribution of ground monitors or a large number of missing values in space due to the influence of clouds. The unique advantage of our seamless day-to-day gaseous pollutant dataset can make up for these shortcomings, allowing us to more accurately and quantitatively assess the changes in gaseous pollutants during the epidemic. We first compared the spatial differences in monthly relative differences from February to April between 2020 and 2019 in China (Figure 4). In February, surface NO_2 sharply reduced in China, especially in key urban agglomerations and megacities, showing relative changes of greater than 50%. A significant decrease in surface SO_2 (> 40%) was observed in northern areas where heavy industry is the mainstay in China (e.g., Tianjin, Hebei, and Shandong), while little change was seen in southern China. Surface CO also showed drastic decreases, but the amplitude was smaller than the other two gaseous pollutants. These were attributed to extensive plant closures and traffic controls due to the lockdown, which started at the end of January 2020, significantly reducing anthropogenic NO_x, SO_2, and CO emissions (Ding et al., 2020; Zheng et al., 2021). In March, surface NO_2 was still generally lower than the historical level in most eastern areas, especially in areas where the epidemic was severe, i.e., Wuhan, Hubei Province, and its surrounding areas. The decrease in surface SO_2 largely slowed by more than two times in the NCP and central China, while surface CO almost returned to normal levels in most areas in China. In April, surface NO_2 and SO_2 were comparable to historical concentrations (within ± 10%), even increasing in some areas of southern and northeastern areas due to rebounding anthropogenic emissions (Ding et al., 2020), especially in Hubei Province, indicating that their surface levels were almost recovered.

[Please insert Figure 4 here]

Most previous studies have focused mainly on changes during the lockdown, with little attention paid to the recovery. We thus compared the time series of daily population-weighted concentrations of the three gaseous pollutants after the Lunar New Year between 2020 and 2019 in China (Figure 5). After the beginning of New Year's Eve, surface gaseous pollutants showed a significant decrease in both the normal and epidemic years due to the closure of factories, with decreasing anthropogenic emissions during the Spring Festival holiday. However, gaseous pollutants in the normal year rose rapidly after they fell to their lowest levels due to the return to work after the holidays. By contrast, their levels continued to decrease in 2020 and were lower than historical levels due to the sustained impacts of the strict lockdowns. They hit bottom in the 4^{th} week after the Lunar New Year, then began to increase gradually. Surface NO_2 and SO_2 recovered in the middle of the 11th week (around the 72nd and 75th days) after the Lunar New Year. However, surface CO levels recovered at the end of the 5th week (around the 34th day), more than twice faster than NO_2 and SO_2 levels. This is attributed to more CO emissions from increased residents' indoor cooking (Zheng et al., 2018), increased atmospheric oxidation capacity (Huang et al., 2020; Wei et al., 2022a), and a potentially higher sensitivity to temperature rises (Lin et al., 2021).

[Please insert Figure 5 here]

3.2.2 Temporal variations and policy implications

Figures S4-S6 show annual mean maps of each gaseous pollutant from 2013 to 2020 in China. Surface NO_2, SO_2, and CO changed greatly, peaking in 2013, with average values of 21.3 ± 8.8 $\mu g/m^3$, 23.1 ± 13.3 $\mu g/m^3$, and 1.01 ± 0.29 mg/m^3, respectively. They reached their lowest levels in 2020, particularly due to the noticeable effects of the COVID-19 epidemic. In general, national ambient NO_2, SO_2, and CO concentrations decreased by approximately 12%, 55%, and 17% from 2013 to 2020, respectively. Large seasonal differences were observed in the amplitude of gaseous pollutant (Figure 6), e.g., surface NO_2 decreased the most in winter, especially in the three urban agglomerations (↓24–31%), changing the least in autumn (especially in the YRD). Surface SO_2 showed much larger decreases in all seasons, especially during the cold seasons (↓55–81%), due to the implementation of stricter “ultra-low” emission standards (Q. Zhang et al., 2019; Li et al., 2022a). Surface CO had similar seasonal changes as SO_2 but 1.5–3.3 times smaller in amplitude.

[Please insert Figure 6 here]

To better investigate the spatiotemporal variations of ambient gaseous pollution, we calculated linear trends and significance levels using monthly anomalies by removing seasonal cycles. Most of China showed significant decreasing trends, with average annual rates of 0.23 $\mu g/m^3$, 2.01 $\mu g/m^3$, and 0.05 mg/m^3 for surface NO_2, SO_2, and CO ($p < 0.001$), respectively (Figure 7), especially in three urban agglomerations and large cities (e.g., Wuhan and Chengdu). The largest downward trends mainly occurred in northern and central China, especially in the BTH (Table 3). This is mainly due to the change in fuel for heating from coal to gas widespread across China in winter (S. Wang et al., 2020), greatly reducing emissions of precursor gases (Koukouli et al., 2018). Increasing trends of surface NO_2 were, however, found in Ningxia and Shanxi Provinces in central China due to increased traffic emissions and new coal-burning power plants in underdeveloped areas without strict regulations on NO_x emissions (van der A et al., 2017; Maji and Sarkar, 2020; C. Li et al., 2022).

We then divided the study period into three periods to investigate the impact of major environmental protection policies on air quality implemented in China (Figure 7). During the Clear Air Action Plan (CAAP, 2013–2017), the rates of decrease for surface NO_2, SO_2, and CO accelerated in most populated areas in China, especially urban areas. This was due to dramatic reductions in main pollutant emissions like SO_2 and NO_x (by 59% and 21%, respectively) through the upgrading of key industries, industrial structure adjustments, and coal-fired boiler remediation (Q. Zhang et al., 2019). In addition, the majority of gaseous pollutants had dropped continuously during the Blue Sky Defense War (BSDW, 2018–2020), benefiting from continuous reductions in total air pollutant emissions and the impacts of COVID-19 (Jiang et al., 2021; Zheng et al., 2021). However, areas with trends passing the significance level sharply shrank, especially for surface SO_2.

During the 13th Five-Year-Plan (FYP, 2016–2020), the decreasing trends of the three gaseous pollutants across China slowed down compared to those during CAAP. Large decreases in surface NO_2 were mainly found in the BTH region and Henan Province, while slightly increasing trends occurred in southern China. Surface SO_2 significantly decreased in most areas, where a greater downward trend was observed in Shanxi Province, mainly due to the reduction in coal consumption thanks to a strengthened clean-heating policy (Lee et al., 2021). Surface CO also continuously decreased, more rapidly in central China but less rapidly elsewhere. The continuous decline in gaseous pollutants is due to the binding reductions in total emissions of major pollutants like NO_x (↓71%) and SO_2 (↓48%) in China (Wan et al., 2022; X. Wu et al., 2022).

[Please insert Figure 7 here]

3.2.3 Population-risk exposure to gaseous pollution

With the daily seamless datasets, we can evaluate the spatial and temporal variations of short-term population-risk exposure to the three gaseous pollutants by calculating the number of days in a given year exceeding the new recommended short-term minimum interim target (IT1) and desired air quality guidelines (AQG) level defined by the WHO in 2021 (WHO, 2021). The area exceeding the recommended levels (i.e., daily NO_2 > 120 μg/m^3, SO_2 > 125 μg/m^3, and CO > 7 mg/m^3) was generally small in eastern China (Figure S7). High NO_2-exposure risks were mainly found in Beijing and Hebei Province and a handful of big cities (e.g., Jinan, Wuhan, Shanghai, and Guangzhou), while high SO_2-exposure risks were mainly observed in Hebei, Shandong, and Shaanxi Provinces. The risk of high CO pollution was small, only found in some scattered areas in the NCP. In general, both the area and the possibility of occurrence exposure to high pollution has gradually decreased over time, almost disappearing since 2018.

By contrast, most areas of eastern China had a surface NO_2 exposure exceeding the AQG level (Figure 8), especially in the north and economically developed areas in the south (proportion > 80%). Both the extent and intensity are decreasing over time, but it is still a problem, suggesting that stronger NO_x controls are needed in the future. Most of the main air pollution transmission belt in China (i.e., the “2 + 26” cities, Figure 1) had surface SO_2 levels exceeding the AQG level at the beginning of the study period. Thanks to strict control measures, these polluted areas sharply decreased after 2015, almost disappearing in 2020. Controlling CO was much more successful in China, with less than 10% of the days in the BTH exceeding the acceptable standard in the early part of the study period. Most areas have reached the CO AQG level since 2018.

[Please insert Figure 8 here]

Figure 9 shows the percentage of days with pollution levels exceeding WHO air quality standards in three key regions. BTH was the only region experiencing high NO_2 and SO_2 exposure risks (i.e., daily mean > IT1), dropping to zero since 2017 and 2016, while YRD and PRD had no high risks of exposure to the three gaseous pollutants (Figure 9a-b). There was also no regional high CO-pollution risk (Figure 9c). However, although declining continuously, regional surface NO_2 levels failed to meet the short-term AQG level in 2020, with 61–73% of the days exceeding the AQG level. More efforts toward mitigating NO_2 levels in these key regions are thus needed. Continual decreases in the number of days above the AQG level were also observed in surface SO_2, reducing to near zero in 2014, 2016, and 2018 in the PRD, YRD, and BTH, respectively. Less than 3% of the days in the BTH and YRD had surface CO levels exceeding the AQG level. Surface CO levels were always below the AQG level in the PRD.

[Please insert Figure 9 here]

3.3 Data quality assessment

Here, the widely used out-of-sample 10-fold cross-validation (10-CV) method was adopted to evaluate the overall estimation accuracy of gaseous pollutants (Rodriguez et al., 2010; Wei et al., 2022a). An additional out-of-station 10-CV approach was used to validate the prediction accuracy of gaseous pollutants, performed based on measurements from ground monitoring stations. These measurements were randomly divided into ten subsets, of which data samples from nine subsets were used for model training and the remaining subset for model validation. This was done 10 times, in turn, to ensure that data from all stations were tested. This procedure generates independent training samples and test samples made in different locations, used to indicate the spatial prediction ability of the model in areas where ground-based measurements are unavailable (S. Wu et al., 2021; Wei et al., 2022a).

3.3.1 Estimate and prediction accuracy

Figure 10 shows the CV results of all daily estimates and predictions for ground-level NO_2, SO_2, and CO concentrations from 2013 to 2020 in China (sample size: $N \approx 3.6$ million). Surface NO_2 and SO_2 concentrations mainly fell in the range of 200 to 500 μg/m^3. Daily estimates were highly correlated to observations, with the same coefficients of determination ($R^2 = 0.84$) and slopes close to 1 (0.86 and 0.84, respectively). Average root-mean-square error (RMSE) [mean absolute error (MAE)] values of surface NO_2 and SO_2 estimates were 7.99 (5.34) and 10.07 (4.68) μg/m^3, and normalized RMSE (NRMSE) values were 0.25 and 0.51, respectively. Most daily CO observations were less than 10 mg/m^3, agreeing well with our daily estimates ($R^2 = 0.80$, slope = 0.79), and the average RMSE (MAE) and NRMSE values were 0.29 (0.16) mg/m^3 and 0.3. Compared to estimation accuracies (Figure 10a-c), prediction accuracies slightly decreased, which is acceptable considering the weak signals of trace gases. Daily surface SO_2, NO_2, and CO predictions (Figure 10d-f) agree well with ground measurements, with spatial R^2 values of 0.70, 0.68, and 0.61, respectively. Their respective RMSE (MAE) values were 14.28 (8.1) μg/m^3, 11.57 (7.06) μg/m^3, and 0.42 (0.24) mg/m^3, and NRMSE values were 0.35, 0.71, and 0.42, respectively, representing the accuracy for areas without ground monitoring stations.

[Please insert Figure 10 here]

The performance of our air pollution modelling was also evaluated on an annual basis, showing that our model works well in estimating and predicting the concentrations of different surface gaseous pollutants in different years (Table 1). The model performance has continuously improved over time, as indicated by increasing correlations and decreasing uncertainties. This is because of the increasing density of ground stations (especially in the suburban areas of cities) and updated quality control of measurements, e.g., improving the sampling flow calibration of monitoring instruments, flow calibration of dynamic calibrators, and revision of precision/accuracy review and data validity judgment (HJ 818-2018) (MEE, 2018b). This has led to an increase in the number of data samples (e.g., from 169 thousand in 2013 to more than 522 thousand in 2020) and improvement in their quality.

[Please insert Table 1 here]

Figure 11 shows the spatial validation of estimated daily pollutant gases across China. In general, our model works well at the site scale, with average CV-R^2 values of 0.77, 0.72, and 0.72, and NRMSE values of 0.25, 0.43, and 0.26 for surface NO_2, SO_2, and CO, respectively. In addition, approximately 93%, 80%, and 84% of the stations had at least moderate agreements (CV-R^2 > 0.6) between our estimates and ground measurements. Except for some scattered sites, the estimation uncertainties were generally less than 0.3, 0.5, and 0.3 in more than 80%, 77%, and 76% of the stations for the above three gaseous pollutant species, respectively.

[Please insert Figure 11 here]

Figure 12 shows the temporal validation of ground-level gaseous pollutants as a function of ground measurements in China. On the monthly scale (Figure 12a-c), we collected a total of ~119,000 matched samples of the three gaseous pollutants. Accuracies significantly improved, with increasing

R^2 (decreasing RMSE) values of 0.93 (4.41 μg/m^3), 0.97 (4.03 μg/m^3), and 0.94 (0.13 mg/m^3) for surface NO_2, SO_2, and CO, respectively. On the annual scale (Figure 12d-f), more than ~10,000 matched samples were collected, showing better agreement with observations (e.g., R^2 = 0.94, 0.98, and 0.97) and lower uncertainties (e.g., RMSE = 3.06 μg/m^3, 2.46 μg/m^3, and 0.07 mg/m^3) for the above three gaseous pollutants, respectively.

[Please insert Figure 12 here]

3.3.2 Comparison with previous studies

We compared our results with those from previous studies on the estimation of the three gaseous pollutants using different developed models focusing on the whole of China. Here, only those studies applying the same out-of-sample cross-validation approach against ground-based measurements collected from the same CNEMC network were selected (Table 2). The statistics shown in the table come from the publications themselves because their generated datasets are not publicly available. We have applied the same validation method and ground measurements as those used in the previous studies. Most generated surface NO_2 datasets had numerous missing values in space limited by direct OMI/Aura satellite observations at spatial resolutions from 0.125°× 0.125° to 0.25°×0.25° (Zhan et al., 2018; Z.-Y. Chen et al., 2019; H. Xu et al., 2019; Chi et al., 2021; Dou et al., 2021). Some studies improved the spatial resolution by introducing NO_2 data from the recently launched Sentinel-5 TROPOMI satellite, but data are only available from October 2018 onward (Liu, 2021; Y. Wang et al., 2021; Chi et al., 2022; Wei et al., 2022b). Surface SO_2 estimated from an SO_2 emission inventory and surface CO from Measurement of Pollution in the Troposphere (MOPITT) and TROPOMI retrievals have a much lower data quality, with smaller R^2 values by 12–57% and larger RMSE values by 41–47% against ground measurements compared to ours (D. Liu et al., 2019; R. Li et al., 2020; Y. Wang et al., 2021). Overall, our gaseous pollutant datasets are superior to those from previous studies in terms of overall accuracy, spatial coverage, and length of data records.

[Please insert Table 2 here]

3.4 Successful applications

Our surface gaseous pollutant datasets have been freely available to the public online since March 2021 (NO_2: https://doi.org/10.5281/zenodo.4641542, SO_2: https://doi.org/10.5281/zenodo.4641538, and CO: https://doi.org/10.5281/zenodo.4641530). A large number of studies have used the three gaseous pollutant datasets generated in this study to study their single or joint impacts on environmental health from both long-term and short-term perspectives, benefiting from the unique daily spatially seamless coverage. For example, a nearly linear relationship between long-term ambient NO_2 and adult mortality in China was observed (Y. Zhang et al., 2022). Y. Wang et al. (2023) reported that ambient NO_2 hindered the survival of middle-aged and elderly people. Long-term SO_2 and CO exposure can increase the incidence rate of visual impairment in children in China (L. Chen et al., 2022a), and short-term exposure to ambient CO can significantly increase the probability of hospitalization for stroke sequelae (R. Wang et al., 2022). Regional and national cohort studies have shown that exposure, especially short-term exposure, to multiple ambient gaseous (NO_2, SO_2, and CO) and particulate pollutants have negative effects of varying degrees on a variety of diseases, like cause-specific cardiovascular disease (R. Xu et al., 2022a,b), ischemic and hemorrhagic stroke (Cai et al., 2022; He et al., 2022; H. Wu et al., 2022b; R. Xu et al., 2022c), asthma mortality (W. Liu et al., 2022), dementia mortality (T. Liu et al., 2022), metabolic syndrome (S. Han et al., 2022), blood pressure (Song et al., 2022; H. Wu et al., 2022a), renal function (S. Li et al., 2022), neurodevelopmental delay (X. Su et al., 2022), serum liver enzymes (Y. Li et al., 2022), overweight and obesity (L. Chen et al., 2022b), insomnia (J. Xu et al., 2021), and sleep quality (L. Wang et al., 2022). These studies attest well to the value of the CHAP dataset regarding current and future public health issues, among others.

4. Summary and conclusions

Exposure to gaseous pollution is detrimental to human health, a major public concern in heavily polluted regions like China, where ground-based observations are not as rich as in major developed countries. Moreover, pollutants travel long distances, affecting large downstream regions. To remedy such limitations, this study applied the machine-learning model called Space-Time Extra-Tree to estimate ambient gaseous pollutants across China, with extensive input variables measured by monitors and satellites, and models. Daily 10 km resolution (approximately 0.1°× 0.1°) seamless (spatial coverage = 100%) datasets for ground-level NO_2, SO_2, and CO concentrations in China from 2013 to 2020 were generated. These datasets were cross-evaluated in terms of overall accuracy and predictive ability at different spatiotemporal levels. National daily estimates (predictions) of surface NO_2, SO_2, and CO were highly consistent with ground measurements, with average out-of-sample (out-of-station) CV-R^2 values of 0.84 (0.68), 0.84 (0.7), and 0.8 (0.61), and RMSEs of 7.99 (11.57) μg/m^3, 10.7 (14.28) μg/m^3, and 0.29 (0.42) mg/m^3, respectively.

Ambient pollutant gases varied significantly in space and time, with high levels mainly found in the North China Plain, especially in winter, due to more anthropogenic emissions, such as coal burning for heating. All gaseous pollutants sharply declined in China during the COVID-19 outbreak, while large differences were observed during their recovery times. For example, surface CO was the first to return to its historical level within the fifth week after the Lunar New Year in 2020, about twice faster as surface NO_2 and SO_2 levels. This is attributed to more home cooking and enhanced atmospheric oxidation. Temporally, surface NO_2, SO_2, and CO levels in China gradually decreased from peaks in 2013 (average = 21.3 ± 8.8 μg/m^3, 23.1 ± 13.3 μg/m^3, and 1.01 ± 0.29 mg/m^3, respectively), with annual rates of decrease of 0.23 μg/m^3, 2.01 μg/m^3, and 0.05 mg/m^3, respectively ($p < 0.001$), until 2020. Improvements in air quality have been made in the last eight years, thanks to the implementation of a series of environmental protection policies, greatly reducing pollutant emissions. In addition, both the areal extents of regions experiencing gaseous pollution and the probability of gaseous pollution occurring have gradually decreased over time, especially for surface CO and SO_2, which have almost reached the short-term air quality guidelines level recommended by the WHO in most areas in China in 2020. This high-quality daily seamless dataset of gaseous pollutants will benefit future environmental and health-related studies focused on China, especially studies investigating short-term air pollution exposure.

Although a lot of new and/or useful data and analyses are presented in this study, they still suffer from some limitations. For example, input variables related to the emission inventory, modeled simulations, and assimilations still have considerable uncertainties. More influential factors stemming from regional economic and development differences need to be considered in more powerful artificial intelligence models to improve the prediction accuracy of air pollutants. The spatiotemporal resolutions of gaseous pollutants will be further improved by integrating information from polar-orbiting and geostationary satellites to investigate diurnal variations. In a future study, we will also reconstruct data records over the last two decades and investigate their long-term spatiotemporal variations, filling the gap of missing observations. This will help us understand their formation mechanisms and impacts on fine particulate matter and ozone pollution in China.

Data availability

CNEMC measurements of gaseous pollutants are available at http://www.cnemc.cn. The reconstructed OMI/Aura tropospheric NO_2 product is available at https://doi.org/10.6084/m9.figshare.13126847. MODIS series products and the MERRA-2 reanalysis are available at https://search.earthdata.nasa.gov/. The SRTM DEM is available at https://www2.jpl.nasa.gov/srtm/, and LandScan™ population information is available at https://landscan.ornl.gov/. The ERA5 reanalysis is available at https://cds.climate.copernicus.eu/, GEOS CF data are available at https://portal.nccs.nasa.gov/datashare/gmao/, and the CAMS reanalysis and emission inventory are available at https://ads.atmosphere.copernicus.eu/.

CHAP dataset availability

The ChinaHighAirPollutants (CHAP) dataset is open access and freely available at https://weijing-rs.github.io/product.html. The ChinaHighNO_2 dataset is available at https://doi.org/10.5281/zenodo.4641542, the ChinaHighSO_2 dataset is available at https://doi.org/10.5281/zenodo.4641538, and the ChinaHighCO dataset is available at https://doi.org/10.5281/zenodo.4641530.

Competing interests

The authors declare that they have no conflict of interest.

Acknowledgments

JW, ZL, and JW were supported by NASA grants 80NSSC21K1980 and 80NSSC19K0950. PG was supported by NASA's Research Opportunities in Space and Earth Science (ROSES-2020), Program Element A.38: Health and Air Quality Applied Sciences Team.

References

Anenberg, S. C., Mohegh, A., Goldberg, D. L., Kerr, G. H., Brauer, M., Burkart, K., Hystad, P., Larkin, A., Wozniak, S., and Lamsal, L.: Long-term trends in urban NO_2 concentrations and associated paediatric asthma incidence: estimates from global datasets, The Lancet Planetary Health, 6, e49-e58, https://doi.org/10.1016/S2542-5196(21)00255-2, 2022.

Cai, M., Zhang, S., Lin, X., Qian, Z., McMillin, S. E., Yang, Y., Zhang, Z., Pan, J., and Lin, H.: Association of ambient particulate matter pollution of different sizes with in-hospital case fatality among stroke patients in China, Neurology, 98(24), e2474-e2486, https://doi.org/10.1212/WNL.0000000000200546, 2022.

Chen, G., Wang, Y., Li, S., Cao, W., Ren, H., Knibbs, L. D., Abramson, M. J., and Guo, Y.: Spatiotemporal patterns of PM_{10} concentrations over China during 2005–2016: a satellite-based estimation using the random forests approach, Environmental Pollution, 242, 605–613, https://doi.org/10.1016/j.envpol.2018.07.012, 2018.

Chen, L., Wei, J., Ma, T., Gao, D., Wang, X., Wen, B., Chen, M., Li, Y., Jiang, J., Wu, L., Li, W., Liu, X., Song, Y., Guo, X., Dong, Y., and Ma, J.: Ambient gaseous pollutant exposure and incidence of visual impairment among children and adolescents: findings from a longitudinal, two-center cohort study in China, Environmental Science and Pollution Research, 29(48), 73,262–73,270, https://doi.org/10.1007/s11356-022-20025-3, 2022a.

Chen, L., Gao, D., Ma, T., Chen, M., Li, Y., Ma, Y., Wen, B., Jiang, J., Wang, X., Zhang, J., Chen, S., Wu, L., Li, W., Liu, X., Guo, X., Huang, S., Wei, J., Song, Y., Ma, J., and Dong, Y.: Could greenness modify the effects of physical activity and air pollutants on overweight and obesity among children and adolescents?, Science of The Total Environment, 832, 155117, https://doi.org/10.1016/j.scitotenv.2022.155117, 2022b.

Chen, Z.-Y., Zhang, R., Zhang, T.-H., Ou, C.-Q., and Guo, Y.: A kriging-calibrated machine learning method for estimating daily ground-level NO_2 in mainland China, Science of The Total Environment, 690, 556–564, https://doi.org/10.1016/j.scitotenv.2019.06.349, 2019.

Chi, Y., Fan, M., Zhao, C., Sun, L., Yang, Y., Yang, X., and Tao, J.: Ground-level NO_2 concentration estimation based on OMI tropospheric NO_2 and its spatiotemporal characteristics in typical regions of China, Atmospheric Research, 264, 105821, https://doi.org/10.1016/j.atmosres.2021.105821, 2021.

Chi, Y., Fan, M., Zhao, C., Yang, Y., Fan, H., Yang, X., Yang, J., and Tao, J.: Machine learning-based estimation of ground-level NO_2 concentrations over China, Science of The Total Environment, 807, 150721, https://doi.org/10.1016/j.scitotenv.2021.150721, 2022.

Cooper, M. J., Martin, R. V., Hammer, M. S., Levelt, P. F., Veefkind, P., Lamsal, L. N., Krotkov, N. A., Brook, J. R., and McLinden, C. A.: Global fine-scale changes in ambient NO_2 during COVID-19 lockdowns, Nature, 601, 380–387, https://doi.org/10.1038/s41586-021-04229-0, 2022.

Dickerson, R. R., Li, C., Li, Z., Marufu, L. T., Stehr, J. W., McClure, B., Krotkov, N., Chen, H., Wang, P., Xia, X., Ban, X., Gong, F., Yuan, J., and Yang, J.: Aircraft observations of dust and pollutants over northeast China: insight into the meteorological mechanisms of transport, 112, https://doi.org/10.1029/2007JD008999, 2007.

Ding, J., van der A, R. J., Eskes, H. J., Mijling, B., Stavrakou, T., van Geffen, J. H. G. M., and Veefkind, J. P.: NO_x emissions reduction and rebound in China due to the COVID-19 crisis, 47, e2020GL089912, https://doi.org/10.1029/2020GL089912, 2020.

Dou, X., Liao, C., Wang, H., Huang, Y., Tu, Y., Huang, X., Peng, Y., Zhu, B., Tan, J., Deng, Z., Wu, N., Sun, T., Ke, P., and Liu, Z.: Estimates of daily ground-level NO_2 concentrations in China based on random forest model integrated k-means, Advances in Applied Energy, 2, 100017, https://doi.org/10.1016/j.adapen.2021.100017, 2021.
Fang, X., Zou, B., Liu, X., Sternberg, T., and Zhai, L.: Satellite-based ground $PM_{2.5}$ estimation using timely structure adaptive modeling, Remote Sensing of Environment, 186, 152–163, https://doi.org/10.1016/j.rse.2016.08.027, 2016.
Field, R. D., Hickman, J. E., Geogdzhayev, I. V., Tsigaridis, K., and Bauer, S. E.: Changes in satellite retrievals of atmospheric composition over eastern China during the 2020 COVID-19 lockdowns, Atmos. Chem. Phys., 21, 18,333–18,350, https://doi.org/10.5194/acp-21-18333-2021, 2021.
Geurts, P., Ernst, D., and Wehenkel, L.: Extremely randomized trees, 36, 3-42, https://doi.org/10.1007/s10994-006-6226-1, 2006.
Han, S., Zhang, F., Yu, H., Wei, J., Xue, L., Duan, Z., and Niu, Z.: Systemic inflammation accelerates the adverse effects of air pollution on metabolic syndrome: findings from the China Health and Retirement Longitudinal Study (CHARLS), Environmental Research, 215, 114340, https://doi.org/10.1016/j.envres.2022.114340, 2022.
Han, W., He, T. L., Tang, Z., Wang, M., Jones, D., and Jiang, Z.: A comparative analysis for a deep learning model (hyDL-CO v1.0) and Kalman filter to predict CO concentrations in China, Geosci. Model Dev., 15, 4225–4237, https://doi.org/10.5194/gmd-15-4225-2022, 2022.
He, F., Wei, J., Dong, Y., Liu, C., Zhao, K., Peng, W., Lu, Z., Zhang, B., Xue, F., Guo, X., and Jia, X.: Associations of ambient temperature with mortality for ischemic and hemorrhagic stroke and the modification effects of greenness in Shandong Province, China, Science of The Total Environment, 158046, https://doi.org/10.1016/j.scitotenv.2022.158046, 2022.
He, J., Gong, S., Yu, Y., Yu, L., Wu, L., Mao, H., Song, C., Zhao, S., Liu, H., Li, X., and Li, R.: Air pollution characteristics and their relation to meteorological conditions during 2014–2015 in major Chinese cities, Environmental Pollution, 223, 484–496, https://doi.org/10.1016/j.envpol.2017.01.050, 2017.
He, L., Wei, J., Wang, Y., Shang, Q., Liu, J., Yin, Y., Frankerberg, C., Jiang, J., Li, Z., and Yung, Y.: Marked impacts of pollution mitigation on crop yields in China. Earth's Future, 10, https://doi.org/10.1029/2022EF002936, 2022.
He, Q., Qin, K., Cohen, J. B., Loyola, D., Li, D., Shi, J., and Xue, Y.: Spatially and temporally coherent reconstruction of tropospheric NO_2 over China combining OMI and GOME-2B measurements, Environmental Research Letters, 15, 125011, https://doi.org/10.1088/1748-9326/abc7df, 2020.
Hersbach, H., Bell, B., Berrisford, P., Hirahara, S., Horányi, A., Muñoz-Sabater, J., Nicolas, J., Peubey, C., Radu, R., Schepers, D., Simmons, A., Soci, C., Abdalla, S., Abellan, X., Balsamo, G., Bechtold, P., Biavati, G., Bidlot, J., Bonavita, M., De Chiara, G., Dahlgren, P., Dee, D., Diamantakis, M., Dragani, R., Flemming, J., Forbes, R., Fuentes, M., Geer, A., Haimberger, L., Healy, S., Hogan, R. J., Hólm, E., Janisková, M., Keeley, S., Laloyaux, P., Lopez, P., Lupu, C., Radnoti, G., de Rosnay, P., Rozum, I., Vamborg, F., Villaume, S., and Thépaut, J.-N.: The ERA5 global reanalysis, 146, 1999–2049, https://doi.org/10.1002/qj.3803, 2020.
Huang, X., Ding, A., Gao, J., Zheng, B., Zhou, D., Qi, X., Tang, R., Wang, J., Ren, C., Nie, W., Chi, X., Xu, Z., Chen, L., Li, Y., Che, F., Pang, N., Wang, H., Tong, D., Qin, W., Cheng, W., Liu,

W., Fu, Q., Liu, B., Chai, F., Davis, S. J., Zhang, Q., and He, K.: Enhanced secondary pollution offset reduction of primary emissions during COVID-19 lockdown in China, National Science Review, 8, https://doi.org/10.1093/nsr/nwaa137, 2020.

Inness, A., Ades, M., Agustí-Panareda, A., Barré, J., Benedictow, A., Blechschmidt, A. M., Dominguez, J. J., Engelen, R., Eskes, H., Flemming, J., Huijnen, V., Jones, L., Kipling, Z., Massart, S., Parrington, M., Peuch, V. H., Razinger, M., Remy, S., Schulz, M., and Suttie, M.: The CAMS reanalysis of atmospheric composition, Atmospheric Chemistry and Physics, 19, 3515–3556, https://doi.org/10.5194/acp-19-3515-2019, 2019.

Jiang, X., Li, G., and Fu, W.: Government environmental governance, structural adjustment and air quality: a quasi-natural experiment based on the Three-year Action Plan to Win the Blue Sky Defense War, Journal of Environmental Management, 277, 111470, https://doi.org/10.1016/j.jenvman.2020.111470, 2021.

Kan, H., Chen, R., and Tong, S.: Ambient air pollution, climate change, and population health in China, Environment International, 42, 10–19, https://doi.org/10.1016/j.envint.2011.03.003, 2012.

Kinney, P. L.: Climate change, air quality, and human health, American Journal of Preventive Medicine, 35, 459–467, https://doi.org/10.1016/j.amepre.2008.08.025, 2008.

Koukouli, M. E., Theys, N., Ding, J., Zyrichidou, I., Mijling, B., Balis, D., and van der A, R. J.: Updated SO_2 emission estimates over China using OMI/Aura observations, Atmospheric Measurement Techniques, 11, 1817–1832, https://doi.org/10.5194/amt-11-1817-2018, 2018.

Lee, E. J., Kim, M. J., and Lee, J.-S.: Policy implications of the clean heating transition: a case study of Shanxi, Energies, 14, 8431, https://doi.org/10.3390/en14248431, 2021.

Levelt, P. F., Stein Zweers, D. C., Aben, I., Bauwens, M., Borsdorff, T., De Smedt, I., Eskes, H. J., Lerot, C., Loyola, D. G., Romahn, F., Stavrakou, T., Theys, N., Van Roozendael, M., Veefkind, J. P., and Verhoelst, T.: Air quality impacts of COVID-19 lockdown measures detected from space using high spatial resolution observations of multiple trace gases from Sentinel-5P/TROPOMI, Atmospheric Chemistry and Physics, 22, 10,319–10,351, https://doi.org/10.5194/acp-22-10319-2022, 2022.

Li, C., Hammer, M. S., Zheng, B., and Cohen, R. C.: Accelerated reduction of air pollutants in China, 2017–2020, Science of The Total Environment, 803, 150011, https://doi.org/10.1016/j.scitotenv.2021.150011, 2022.

Li, R., Wang, Z., Cui, L., Fu, H., Zhang, L., Kong, L., Chen, W., and Chen, J.: Air pollution characteristics in China during 2015–2016: spatiotemporal variations and key meteorological factors, Science of The Total Environment, 648, 902–915, https://doi.org/10.1016/j.scitotenv.2018.08.181, 2019.

Li, R., Cui, L., Liang, J., Zhao, Y., Zhang, Z., and Fu, H.: Estimating historical SO_2 level across the whole China during 1973–2014 using random forest model, Chemosphere, 247, 125839, https://doi.org/10.1016/j.chemosphere.2020.125839, 2020.

Li, S., Meng, Q., Laba, C., Guan, H., Wang, Z., Pan, Y., Wei, J., Xu, H., Zeng, C., Wang, X., Jiang, M., Lu, R., Guo, B., and Zhao, X.: Associations between long-term exposure to ambient air pollution and renal function in Southwest China: The China Multi-Ethnic Cohort (CMEC) study, Ecotoxicology and Environmental Safety, 242, 113851, https://doi.org/10.1016/j.ecoenv.2022.113851, 2022.

Li, T., Shen, H., Yuan, Q., Zhang, X., and Zhang, L.: Estimating ground-level $PM_{2.5}$ by fusing satellite and station observations: a geo-intelligent deep learning approach, 44, 11,985–911,993, https://doi.org/10.1002/2017GL075710, 2017.

Li, Y., Yuan, X., Wei, J., Sun, Y., Ni, W., Zhang, H., Zhang, Y., Wang, R., Xu, R., Liu, T., Yang, C., Chen, G., Xu, J., and Liu, Y.: Long-term exposure to ambient air pollution and serum liver enzymes in older adults: a population-based longitudinal study, Annals of Epidemiology, 74, 1–7, https://doi.org/10.1016/j.annepidem.2022.05.011, 2022.

Li, Z., Guo, J., Ding, A., Liao, H., Liu, J., Sun, Y., Wang, T., Xue, H., Zhang, H., and Zhu, B.: Aerosol and boundary-layer interactions and impact on air quality, National Science Review, 4, 810–833, https://doi.org/10.1093/nsr/nwx117, 2017.

Lin, J., Lin, C., Tao, M., Ma, J., Fan, L., Xu, R.-A., and Fang, C.: Spatial disparity of meteorological impacts on carbon monoxide pollution in China during the COVID-19 lockdown period, ACS Earth and Space Chemistry, 5, 2900–2909, https://doi.org/10.1021/acsearthspacechem.1c00251, 2021.

Ling, C. and Li, Y.: Substantial changes of gaseous pollutants and health effects during the COVID-19 lockdown period across China, GeoHealth, 5, e2021GH000408, https://doi.org/10.1029/2021GH000408, 2021.

Liu, J.: Mapping high resolution national daily NO_2 exposure across mainland China using an ensemble algorithm, Environmental Pollution, 279, 116932, https://doi.org/10.1016/j.envpol.2021.116932, 2021.

Liu, D., Di, B., Luo, Y., Deng, X., Zhang, H., Yang, F., Grieneisen, M. L., and Zhan, Y.: Estimating ground-level CO concentrations across China based on the national monitoring network and MOPITT: potentially overlooked CO hotspots in the Tibetan Plateau, Atmospheric Chemistry and Physics, 19, 12,413–12,430, https://doi.org/10.5194/acp-19-12413-2019, 2019.

Liu, T., Zhou, Y., Wei, J., Chen, Q., Xu, R., Pan, J., Lu, W., Wang, Y., Fan, Z., Li, Y., Xu, L., Cui, X., Shi, C., Zhang, L., Chen, X., Bao, W., Sun, H., and Liu, Y.: Association between short-term exposure to ambient air pollution and dementia mortality in Chinese adults, Science of The Total Environment, 849, 157860, https://doi.org/10.1016/j.scitotenv.2022.157860, 2022.

Liu, W., Wei, J., Cai, M., Qian, Z., Long, Z., Wang, L., Vaughn, M. G., Aaron, H. E., Tong, X., Li, Y., Yin, P., Lin, H., and Zhou, M.: Particulate matter pollution and asthma mortality in China: a nationwide time-stratified case-crossover study from 2015 to 2020, Chemosphere, 308, 136316, https://doi.org/10.1016/j.chemosphere.2022.136316, 2022.

Ma, Z., Dey, S., Christopher, S., Liu, R., Bi, J., Balyan, P., and Liu, Y.: A review of statistical methods used for developing large-scale and long-term $PM_{2.5}$ models from satellite data, Remote Sensing of Environment, 269, 112827, https://doi.org/10.1016/j.rse.2021.112827, 2022.

Maji, K. J. and Sarkar, C.: Spatio-temporal variations and trends of major air pollutants in China during 2015–2018, Environmental Science and Pollution Research, 27, 33,792-33,808, https://doi.org/10.1007/s11356-020-09646-8, 2020.

MEE: Technical regulation for selection of ambient air quality monitoring stations (on trial) (in Chinese), Ministry of Ecology and Environment of the People's Republic of China, available at: https://www.mee.gov.cn/ywgz/fgbz/bz/bzwb/jcffbz/201309/W020131105548727856307.pdf, 2013a.

MEE: Specifications and test procedures for ambient air quality continuous automated monitoring system for SO_2, NO_2, O_3 and CO (HJ 654-2013) (in Chinese), Ministry of Ecology and Environment of the People's Republic of China, available at: https://www.mee.gov.cn/ywgz/fgbz/bz/bzwb/jcffbz/201308/t20130802_20256853.shtml, 2013b.

MEE: Technical specifications for installation and acceptance of ambient air quality continuous automated monitoring system for SO_2, NO_2, O_3 and CO (HJ 193-2013) (in English), Ministry of Ecology and Environment of the People's Republic of China, https://english.mee.gov.cn/Resources/standards/Air_Environment/air_method/201308/t20130816_257560.shtm, 2013c.

MEE: Revision of the ambient air quality standards (GB 3095-2012) (in Chinese), Ministry of Ecology and Environment of the People's Republic of China, available at: http://www.mee.gov.cn/xxgk2018/xxgk/xxgk2001/201808/t20180815_20629602.html, 2018a.

MEE: Technical specifications for operation and quality control of ambient air quality continuous automated monitoring system for SO_2, NO_2, O_3 and CO (HJ 818-2018) (in Chinese), Ministry of Ecology and Environment of the People's Republic of China, available at: http://www.cnemc.cn/jcgf/dqhj/202009/t20200922_20799646.shtml, 2018b.

Muñoz-Sabater, J., Dutra, E., Agustí-Panareda, A., Albergel, C., Arduini, G., Balsamo, G., Boussetta, S., Choulga, M., Harrigan, S., Hersbach, H., Martens, B., Miralles, D. G., Piles, M., Rodríguez-Fernández, N. J., Zsoter, E., Buontempo, C., and Thépaut, J. N.: ERA5-Land: a state-of-the-art global reanalysis dataset for land applications, Earth System Science Data, 13, 4349–4383, https://doi.org/10.5194/essd-13-4349-2021, 2021.

Murray, C. J. L., Aravkin, A. Y., Zheng, P., and Coauthors: Global burden of 87 risk factors in 204 countries and territories, 1990–2019: a systematic analysis for the Global Burden of Disease Study 2019, The Lancet, 396, 1223–1249, https://doi.org/10.1016/S0140-6736(20)30752-2, 2020.

Orellano, P., Reynoso, J., Quaranta, N., Bardach, A., and Ciapponi, A.: Short-term exposure to particulate matter (PM_{10} and $PM_{2.5}$), nitrogen dioxide (NO_2), and ozone (O_3) and all-cause and cause-specific mortality: systematic review and meta-analysis, Environment International, 142, 105876, https://doi.org/10.1016/j.envint.2020.105876, 2020.

Qin, K., Rao, L., Xu, J., Bai, Y., Zou, J., Hao, N., Li, S., and Yu, C.: Estimating ground level NO_2 concentrations over central-eastern China using a satellite-based geographically and temporally weighted regression model, Remote Sensing, 9, 950, https://doi.org/10.3390/rs9090950, 2017.

Rodriguez, J. D., Perez, A., and Lozano, J. A.: Sensitivity analysis of k-fold cross validation in prediction error estimation, IEEE Transactions on Pattern Analysis and Machine Intelligence, 32, 569–575, https://doi.org/10.1109/TPAMI.2009.187, 2010.

Seo, J., Kim, J. Y., Youn, D., Lee, J. Y., Kim, H., Lim, Y. B., Kim, Y., and Jin, H. C.: On the multiday haze in the Asian continental outflow: the important role of synoptic conditions combined with regional and local sources, Atmospheric Chemistry and Physics, 17, 9311–9332, https://doi.org/10.5194/acp-17-9311-2017, 2017.

Shah, V., Jacob, D. J., Li, K., Silvern, R. F., Zhai, S., Liu, M., Lin, J., and Zhang, Q.: Effect of changing NO_x lifetime on the seasonality and long-term trends of satellite-observed tropospheric NO_2 columns over China, Atmospheric Chemistry and Physics, 20, 1483–1495, https://doi.org/10.5194/acp-20-1483-2020, 2020.

Song, J., Du, P., Yi, W., Wei, J., Fang, J., Pan, R., Zhao, F., Zhang, Y., Xu, Z., Sun, Q., Liu, Y., Chen, C., Cheng, J., Lu, Y., Li, T., Su, H., and Shi, X.: Using an exposome-wide approach to explore the impact of urban environments on blood pressure among adults in Beijing–Tianjin–Hebei and surrounding areas of China, Environmental Science & Technology, 56, 8395–8405, https://doi.org/10.1021/acs.est.1c08327, 2022.

Su, T., Li, Z., Zheng, Y., Luan, Q., and Guo, J.: Abnormally shallow boundary layer associated with severe air pollution during the COVID-19 lockdown in China, Geophysical Research Letters, 47, e2020GL090041, https://doi.org/10.1029/2020GL090041, 2020.

Su, X., Zhang, S., Lin, Q., Wu, Y., Yang, Y., Yu, H., Huang, S., Luo, W., Wang, X., Lin, H., Ma, L., and Zhang, Z.: Prenatal exposure to air pollution and neurodevelopmental delay in children: a birth cohort study in Foshan, China, Science of The Total Environment, 816, 151658, https://doi.org/10.1016/j.scitotenv.2021.151658, 2022.

Sun, Q., Hong, X., and Wold, L. E.: Cardiovascular effects of ambient particulate air pollution exposure, 121, 2755–2765, https://doi.org/10.1161/CIRCULATIONAHA.109.893461, 2010.

Tian, H., Liu, Y., Li, Y., Wu, C.-H., Chen, B., Kraemer, M. U. G., Li, B., Cai, J., Xu, B., Yang, Q., Wang, B., Yang, P., Cui, Y., Song, Y., Zheng, P., Wang, Q., Bjornstad, O. N., Yang, R., Grenfell, B. T., Pybus, O. G., and Dye, C.: An investigation of transmission control measures during the first 50 days of the COVID-19 epidemic in China, Science, 368, 638–642, https://doi.org/10.1126/science.abb6105, 2020.

van der A, R. J., Mijling, B., Ding, J., Koukouli, M. E., Liu, F., Li, Q., Mao, H., and Theys, N.: Cleaning up the air: effectiveness of air quality policy for SO_2 and NO_x emissions in China, Atmospheric Chemistry and Physics, 17, 1775–1789, https://doi.org/10.5194/acp-17-1775-2017, 2017.

Wan, J., Qin, C., Wang, Q., Xiao, Y., Niu, R., Li, X., and Su, J.: A brief overview of the 13th Five-Year Plan for the protection of ecological environment, in: Environmental Strategy and Planning in China, edited by: Wang, J., Wang, X., and Wan, J., Springer Singapore, Singapore, 57–85, https://doi.org/10.1007/978-981-16-6909-5_3, 2022.

Wang, L., Zhang, J., Wei, J., Zong, J., Lu, C., Du, Y., and Wang, Q.: Association of ambient air pollution exposure and its variability with subjective sleep quality in China: a multilevel modeling analysis, Environmental Pollution, 312, 120020, https://doi.org/10.1016/j.envpol.2022.120020, 2022.

Wang, R., Xu, R., Wei, J., Liu, T., Ye, Y., Li, Y., Lin, Q., Zhou, Y., Huang, S., Lv, Z., Tian, Q., and Liu, Y.: Short-term exposure to ambient air pollution and hospital admissions for sequelae of stroke in Chinese older adults, GeoHealth, 6, e2022GH000700, https://doi.org/10.1029/2022GH000700, 2022.

Wang, S., Su, H., Chen, C., Tao, W., Streets, D. G., Lu, Z., Zheng, B., Carmichael, G. R., Lelieveld, J., Pöschl, U., and Cheng, Y.: Natural gas shortages during the "coal-to-gas" transition in China have caused a large redistribution of air pollution in winter 2017, Proceedings of the National Academy of Sciences, 117, 31,018–31,025, https://doi.org/10.1073/pnas.2007513117, 2020.

Wang, Y., Yuan, Q., Li, T., Zhu, L., and Zhang, L.: Estimating daily full-coverage near surface O_3, CO, and NO_2 concentrations at a high spatial resolution over China based on S5P-TROPOMI and GEOS-FP, ISPRS Journal of Photogrammetry and Remote Sensing, 175, 311–325, https://doi.org/10.1016/j.isprsjprs.2021.03.018, 2021.

Wang, Y., Ma, Y. F., Eskes, H., Inness, A., Flemming, J., and Brasseur, G. P.: Evaluation of the

CAMS global atmospheric trace gas reanalysis 2003–2016 using aircraft campaign observations, Atmospheric Chemistry and Physics, 20, 4493–4521, 10.5194/acp-20-4493-2020, 2020.

Wang, Y., Luo, S., Wei, J., Yang, Z., Hu, K., Yao, Y., and Zhang, Y.: Ambient NO_2 exposure hinders long-term survival of Chinese middle-aged and older adults, Science of The Total Environment, 855, 158784, https://doi.org/10.1016/j.scitotenv.2022.158784, 2023.

Wei, J., Li, Z., Guo, J., Sun, L., Huang, W., Xue, W., Fan, T., and Cribb, M.: Satellite-derived 1-km-resolution PM_1 concentrations from 2014 to 2018 across China, Environmental Science & Technology, 53, 13,265–13,274, https://doi.org/10.1021/acs.est.9b03258, 2019.

Wei, J., Li, Z., Cribb, M., Huang, W., Xue, W., Sun, L., Guo, J., Peng, Y., Li, J., Lyapustin, A., Liu, L., Wu, H., and Song, Y.: Improved 1-km resolution $PM_{2.5}$ estimates across China using enhanced space–time extremely randomized trees, Atmospheric Chemistry and Physics, 20, 3273–3289, https://doi.org/10.5194/acp-20-3273-2020, 2020.

Wei, J., Li, Z., Lyapustin, A., Sun, L., Peng, Y., Xue, W., Su, T., and Cribb, M.: Reconstructing 1-km-resolution high-quality $PM_{2.5}$ data records from 2000 to 2018 in China: spatiotemporal variations and policy implications, Remote Sensing of Environment, 252, 112136, https://doi.org/10.1016/j.rse.2020.112136, 2021a.

Wei, J., Li, Z., Xue, W., Sun, L., Fan, T., Liu, L., Su, T., and Cribb, M.: The ChinaHighPM10 dataset: generation, validation, and spatiotemporal variations from 2015 to 2019 across China, Environment International, 146, 106290, https://doi.org/10.1016/j.envint.2020.106290, 2021b.

Wei, J., Li, Z., Li, K., Dickerson, R. R., Pinker, R. T., Wang, J., Liu, X., Sun, L., Xue, W., and Cribb, M.: Full-coverage mapping and spatiotemporal variations of ground-level ozone (O_3) pollution from 2013 to 2020 across China, Remote Sensing of Environment, 270, 112775, https://doi.org/10.1016/j.rse.2021.112775, 2022a.

Wei, J., Liu, S., Li, Z., Liu, C., Qin, K., Liu, X., Pinker, R. T., Dickerson, R. R., Lin, J., Boersma, K. F., Sun, L., Li, R., Xue, W., Cui, Y., Zhang, C., and Wang, J.: Ground-level NO_2 surveillance from space across China for high resolution using interpretable spatiotemporally weighted artificial intelligence, Environmental Science & Technology, 56, 9988–9998, https://doi.org/10.1021/acs.est.2c03834, 2022b.

WHO: Coronavirus Disease (COVID-19) Pandemic, The World Health Organization, available online: https://www.who.int/emergencies/diseases/novel-coronavirus-2019, 2020.

WHO: WHO global air quality guidelines. Particulate matter ($PM_{2.5}$ and PM_{10}), ozone, nitrogen dioxide, sulfur dioxide and carbon monoxide, Geneva: World Health Organization, Licence: CC BY-NC-SA 3.0 IGO, Licence: CC BY-NC-SA 3.0 IGO, 2021.

Wu, H., Zhang, Y., Zhao, M., Liu, W., Magnussen, C. G., Wei, J., and Xi, B.: Short-term effects of exposure to ambient PM_1 on blood pressure in children and adolescents aged 9 to 18 years in Shandong Province, China, Atmospheric Environment, 283, 119180, https://doi.org/10.1016/j.atmosenv.2022.119180, 2022a.

Wu, H., Lu, Z., Wei, J., Zhang, B., Liu, X., Zhao, M., Liu, W., Guo, X., and Xi, B.: Effects of the COVID-19 lockdown on air pollutant levels and associated reductions in ischemic stroke incidence in Shandong Province, China, Frontiers in Public Health, 10, https://doi.org/10.3389/fpubh.2022.876615, 2022b.

Wu, S., Huang, B., Wang, J., He, L., Wang, Z., Yan, Z., Lao, X., Zhang, F., Liu, R., and Du, Z.: Spatiotemporal mapping and assessment of daily ground NO_2 concentrations in China using high-resolution TROPOMI retrievals, Environmental Pollution, 273, 116456, https://doi.org/10.1016/j.envpol.2021.116456, 2021.

Wu, X., Yang, Y., Gong, Y., Deng, Z., Wang, Y., Wu, W., Zheng, C., and Zhang, Y.: Advances in air pollution control for key industries in China during the 13th Five-Year Plan, Journal of Environmental Sciences, https://doi.org/10.1016/j.jes.2022.09.008, 2022.

Xu, H., Bechle, M. J., Wang, M., Szpiro, A. A., Vedal, S., Bai, Y., and Marshall, J. D.: National $PM_{2.5}$ and NO_2 exposure models for China based on land use regression, satellite measurements, and universal kriging, Science of The Total Environment, 655, 423–433, https://doi.org/10.1016/j.scitotenv.2018.11.125, 2019.

Xu, J., Zhou, J., Luo, P., Mao, D., Xu, W., Nima, Q., Cui, C., Yang, S., Ao, L., Wu, J., Wei, J., Chen, G., Li, S., Guo, Y., Zhang, J., Liu, Z., and Zhao, X.: Associations of long-term exposure to ambient air pollution and physical activity with insomnia in Chinese adults, Science of The Total Environment, 792, 148197, https://doi.org/10.1016/j.scitotenv.2021.148197, 2021.

Xu, R., Wei, J., Liu, T., Li, Y., Yang, C., Shi, C., Chen, G., Zhou, Y., Sun, H., and Liu, Y.: Association of short-term exposure to ambient PM_1 with total and cause-specific cardiovascular disease mortality, Environment International, 169, 107519, https://doi.org/10.1016/j.envint.2022.107519, 2022a.

Xu, R., Shi, C., Wei, J., Lu, W., Li, Y., Liu, T., Wang, Y., Zhou, Y., Chen, G., Sun, H., and Liu, Y.: Cause-specific cardiovascular disease mortality attributable to ambient temperature: a time-stratified case-crossover study in Jiangsu province, China, Ecotoxicology and Environmental Safety, 236, 113498, https://doi.org/10.1016/j.ecoenv.2022.113498, 2022b.

Xu, R., Wang, Q., Wei, J., Lu, W., Wang, R., Liu, T., Wang, Y., Fan, Z., Li, Y., Xu, L., Shi, C., Li, G., Chen, G., Zhang, L., Zhou, Y., Liu, Y., and Sun, H.: Association of short-term exposure to ambient air pollution with mortality from ischemic and hemorrhagic stroke, European Journal of Neurology, 29, 1994–2005, https://doi.org/10.1111/ene.15343, 2022c.

Xu, W. Y., Zhao, C. S., Ran, L., Deng, Z. Z., Liu, P. F., Ma, N., Lin, W. L., Xu, X. B., Yan, P., He, X., Yu, J., Liang, W. D., and Chen, L. L.: Characteristics of pollutants and their correlation to meteorological conditions at a suburban site in the North China Plain, Atmospheric Chemistry and Physics, 11, 4353–4369, https://doi.org/10.5194/acp-11-4353-2011, 2011.

Yoo, J.-M., Lee, Y.-R., Kim, D., Jeong, M.-J., Stockwell, W. R., Kundu, P. K., Oh, S.-M., Shin, D.-B., and Lee, S.-J.: New indices for wet scavenging of air pollutants (O_3, CO, NO_2, SO_2, and PM_{10}) by summertime rain, Atmospheric Environment, 82, 226–237, https://doi.org/10.1016/j.atmosenv.2013.10.022, 2014.

Zhan, Y., Luo, Y., Deng, X., Zhang, K., Zhang, M., Grieneisen, M. L., and Di, B.: Satellite-based estimates of daily NO_2 exposure in China using hybrid random forest and spatiotemporal kriging model, Environmental Science & Technology, 52, 4180–4189, https://doi.org/10.1021/acs.est.7b05669, 2018.

Zhang, B., Rong, Y., Yong, R., Qin, D., Li, M., Zou, G., and Pan, J.: Deep learning for air pollutant concentration prediction: a review, Atmospheric Environment, 290, 119347, https://doi.org/10.1016/j.atmosenv.2022.119347, 2022.

Zhang, C., Liu, C., Hu, Q., Cai, Z., Su, W., Xia, C., Zhu, Y., Wang, S., and Liu, J.: Satellite UV-Vis spectroscopy: implications for air quality trends and their driving forces in China during 2005–2017, Light: Science & Applications, 8, 100, 10.1038/s41377-019-0210-6, 2019.

Zhang, Q., Zheng, Y., Tong, D., Shao, M., Wang, S., Zhang, Y., Xu, X., Wang, J., He, H., Liu, W., Ding, Y., Lei, Y., Li, J., Wang, Z., Zhang, X., Wang, Y., Cheng, J., Liu, Y., Shi, Q., Yan, L., Geng, G., Hong, C., Li, M., Liu, F., Zheng, B., Cao, J., Ding, A., Gao, J., Fu, Q., Huo, J., Liu, B., Liu, Z., Yang, F., He, K., and Hao, J.: Drivers of improved $PM_{2.5}$ air quality in China from 2013 to 2017, Proceedings of the National Academy of Sciences, 116, 24,463–24,469, https://doi.org/10.1073/pnas.1907956116, 2019.

Zhang, Y., Li, Z., Wei, J., Zhan, Y., Liu, L., Yang, Z., Zhang, Y., Liu, R., and Ma, Z.: Long-term exposure to ambient NO_2 and adult mortality: a nationwide cohort study in China, Journal of Advanced Research, 41, 13–22, https://doi.org/10.1016/j.jare.2022.02.007, 2022.

Zhang, Z., Wang, J., Hart, J. E., Laden, F., Zhao, C., Li, T., Zheng, P., Li, D., Ye, Z., and Chen, K.: National scale spatiotemporal land-use regression model for $PM_{2.5}$, PM_{10} and NO_2 concentration in China, Atmospheric Environment, 192, 48–54, https://doi.org/10.1016/j.atmosenv.2018.08.046, 2018.

Zheng, B., Chevallier, F., Ciais, P., Yin, Y., Deeter, M. N., Worden, H. M., Wang, Y., Zhang, Q., and He, K.: Rapid decline in carbon monoxide emissions and export from East Asia between years 2005 and 2016, Environmental Research Letters, 13, 044007, https://doi.org/10.1088/1748-9326/aab2b3, 2018.

Zheng, B., Zhang, Q., Geng, G., Chen, C., Shi, Q., Cui, M., Lei, Y., and He, K.: Changes in China's anthropogenic emissions and air quality during the COVID-19 pandemic in 2020, Earth System Science Data, 13, 2895–2907, https://doi.org/10.5194/essd-13-2895-2021, 2021.

Figures

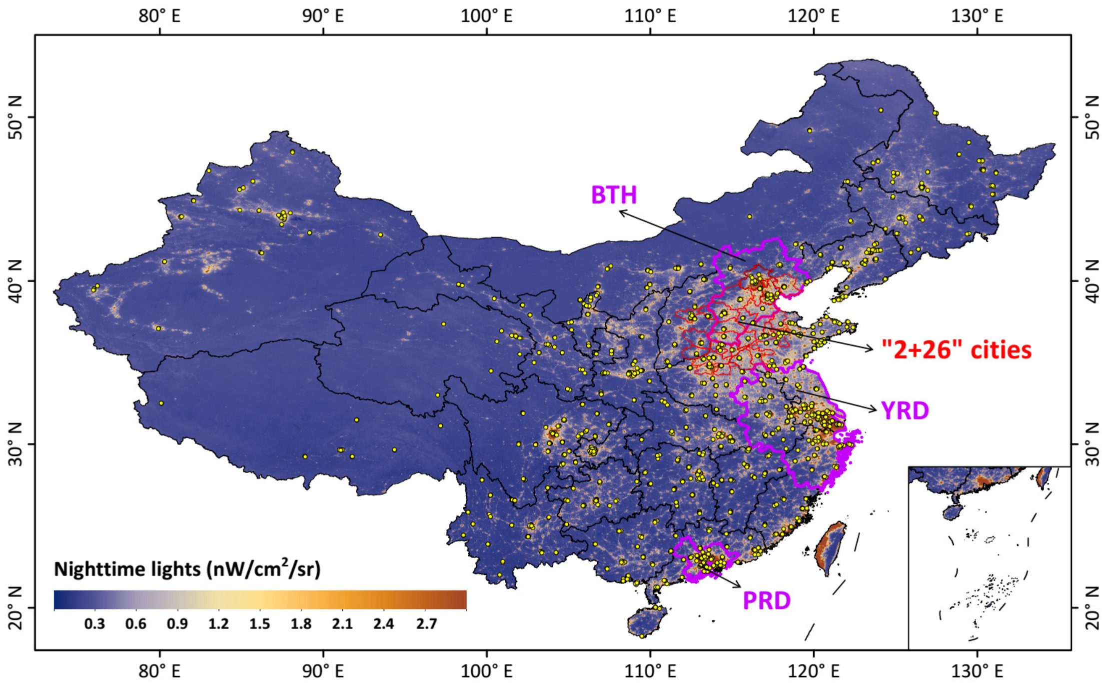

Figure 1. Geographical locations of ground-based stations from the China National Environmental Monitoring Centre network (marked as yellow dots) monitoring gaseous pollutants across China. The background shows the nighttime-light level, an estimate of population. Purple boundaries three typical urban agglomerations: the Beijing-Tianjin-Hebei (BTH) region, the Yangtze River Delta (YRD), and the Pearl River Delta (PRD).

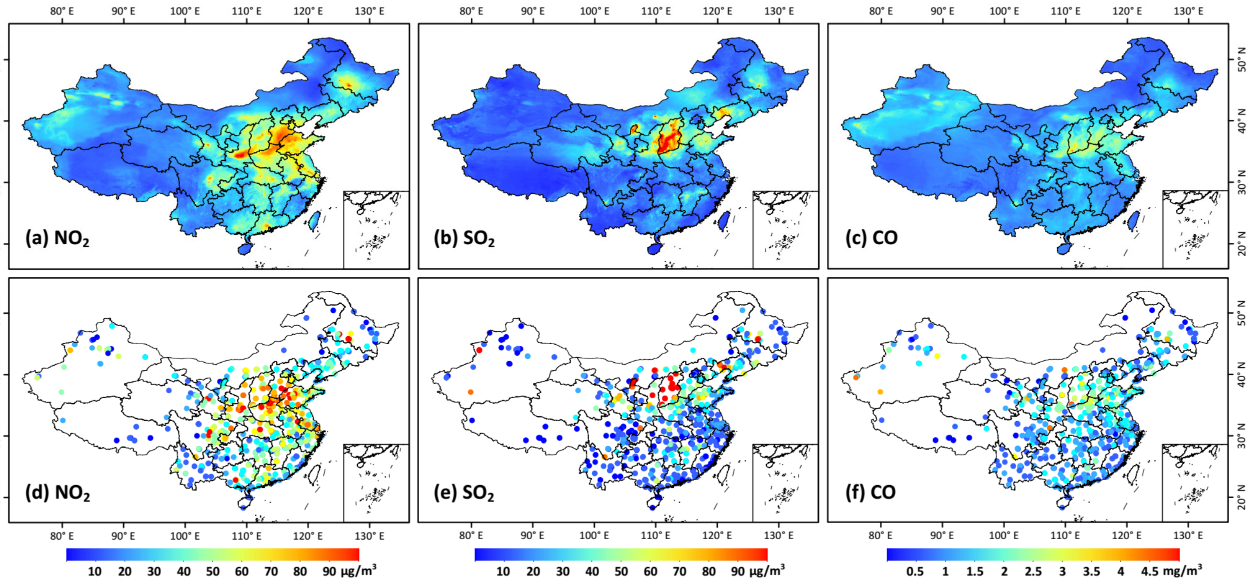

Figure 2. A typical example of (a-c) big-data-derived (horizontal resolution = 10 km) seamless surface NO_2 ($\mu g/m^3$), SO_2 ($\mu g/m^3$), and CO (mg/m^3) concentrations and (d-f) corresponding ground measurements on 1 January 2018 in China.

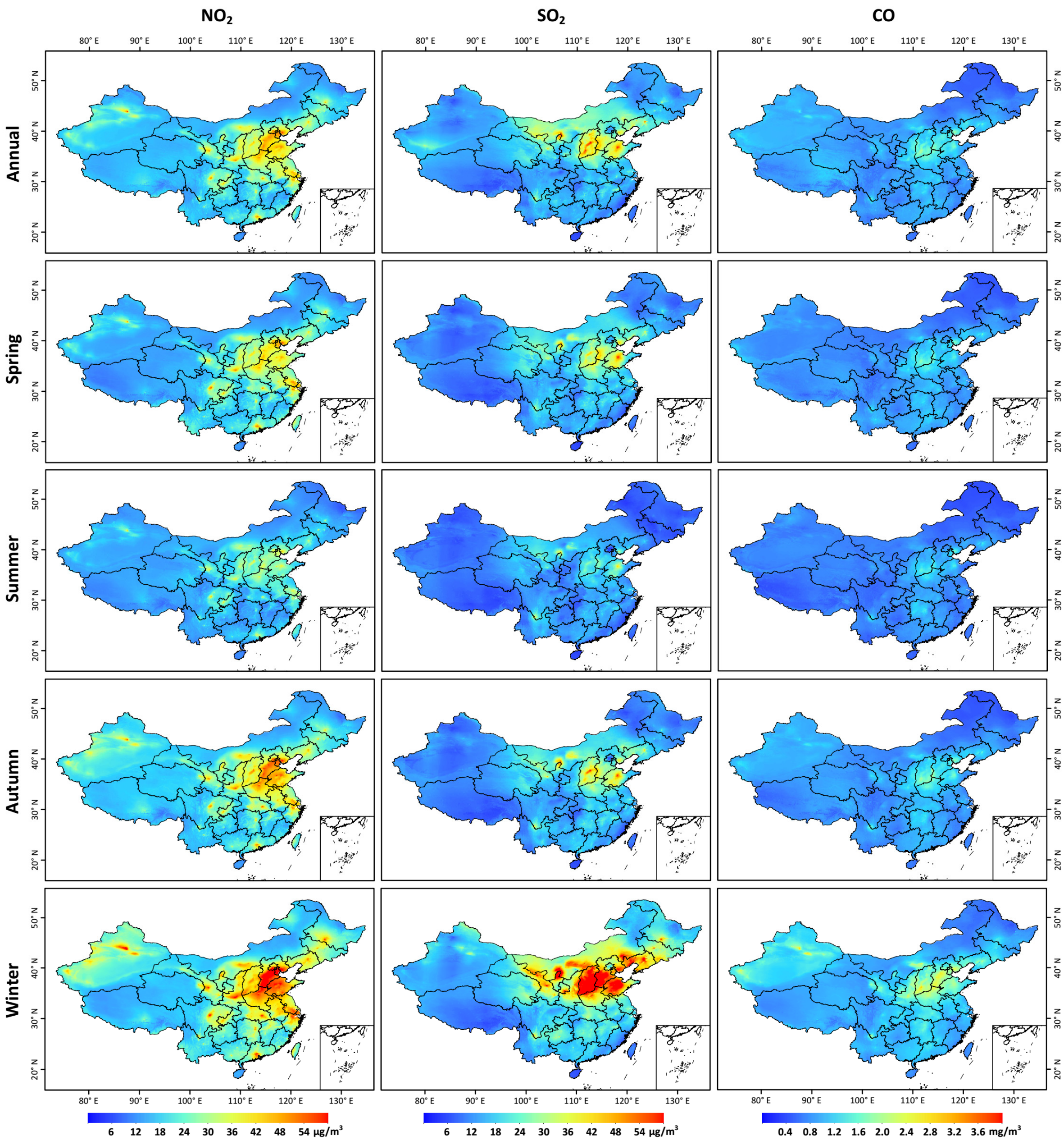

Figure 3. Annual and seasonal mean maps (horizontal resolution = 10 km) of surface NO_2 ($\mu g/m^3$), SO_2 ($\mu g/m^3$), and CO (mg/m^3) averaged over the period 2013–2020 in China.

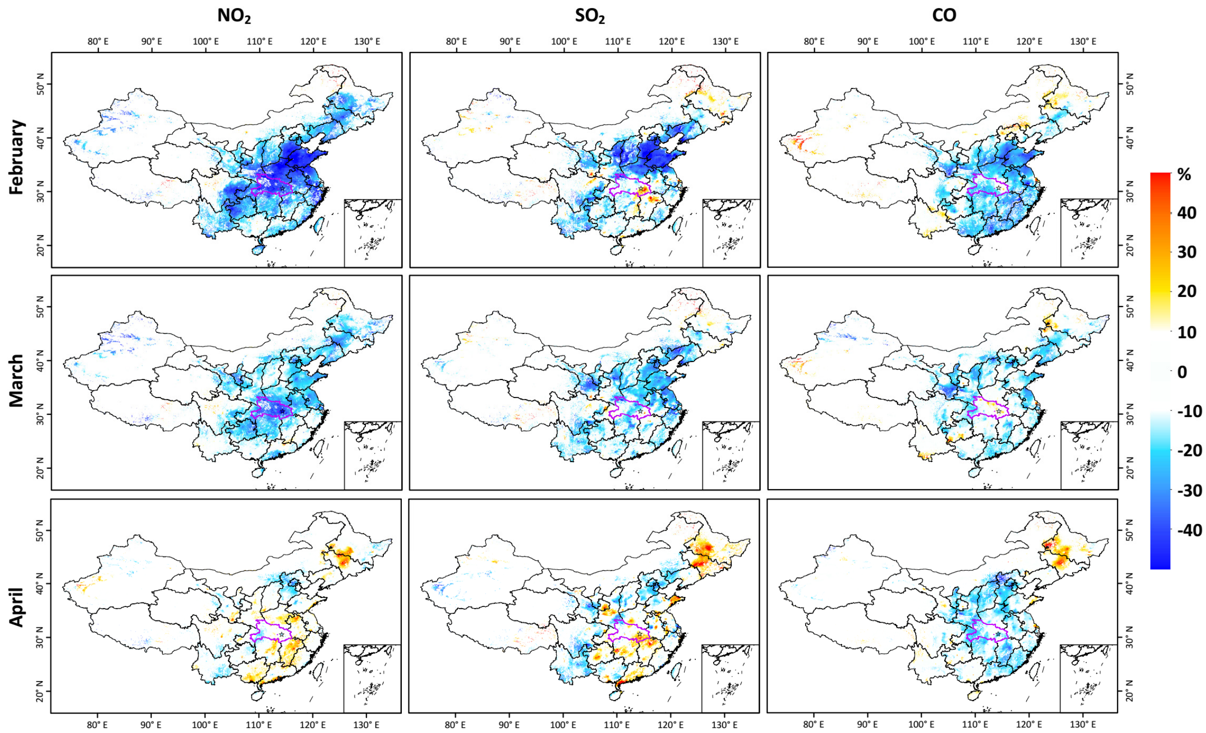

Figure 4. Relative changes (%) in surface NO_2, SO_2, and CO concentrations in February, March, and April between 2019 and 2020 in populated areas of China. The area outlined in magenta and the star in each panel indicate Hubei Province and Wuhan City, respectively.

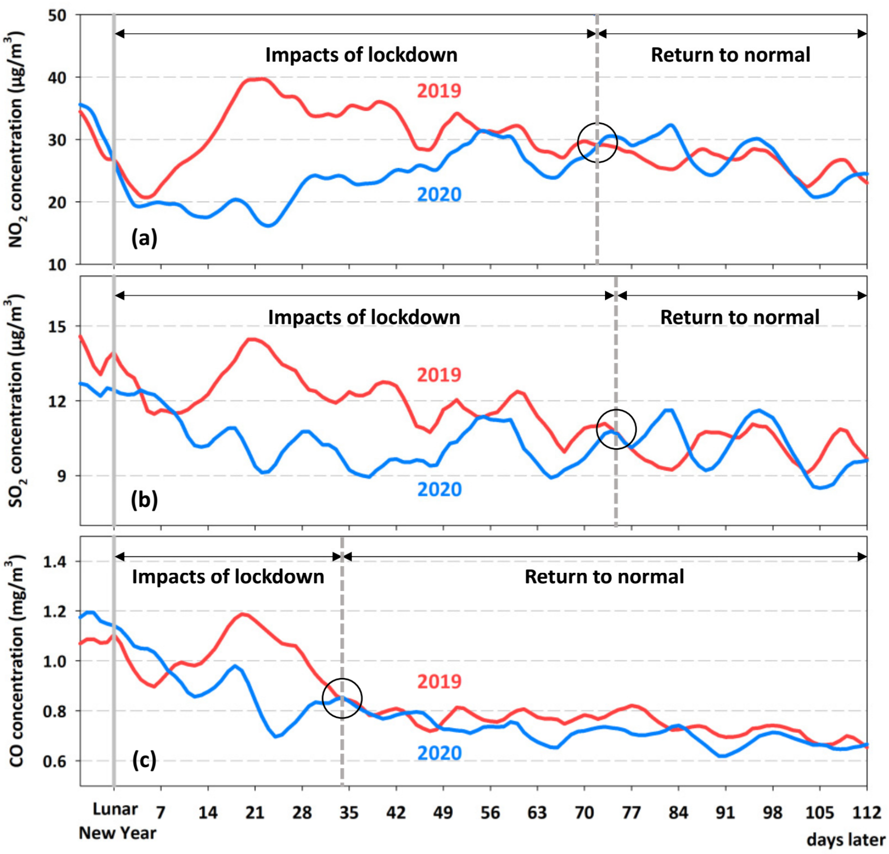

Figure 5. Time series of the seven-day moving averages of daily population-weighted surface (a) NO_2, (b) SO_2, and (c) CO concentrations after the Lunar New Year of 2019 and 2020 in China. The black circle in each panel shows the turning point when the gaseous pollutants began to return to their normal levels.

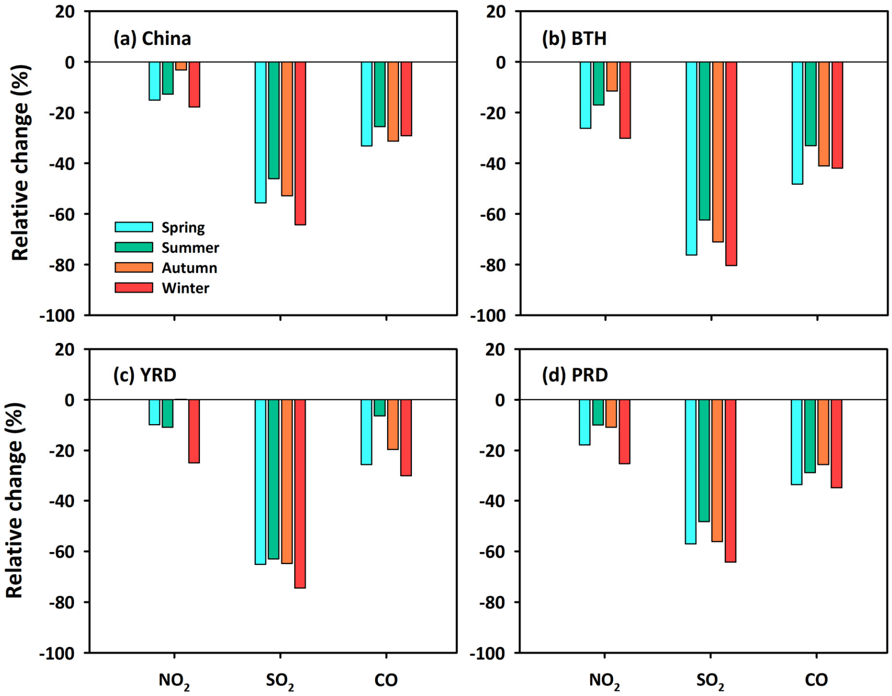

Figure 6. Relative changes (%) in seasonal mean surface NO_2, SO_2, and CO concentrations between 2013 and 2020 over (a) China, (b) the Beijing-Tianjin-Hebei (BTH) region, (c) the Yangtze River Delta (YRD), and (d) the Pearl River Delta (PRD).

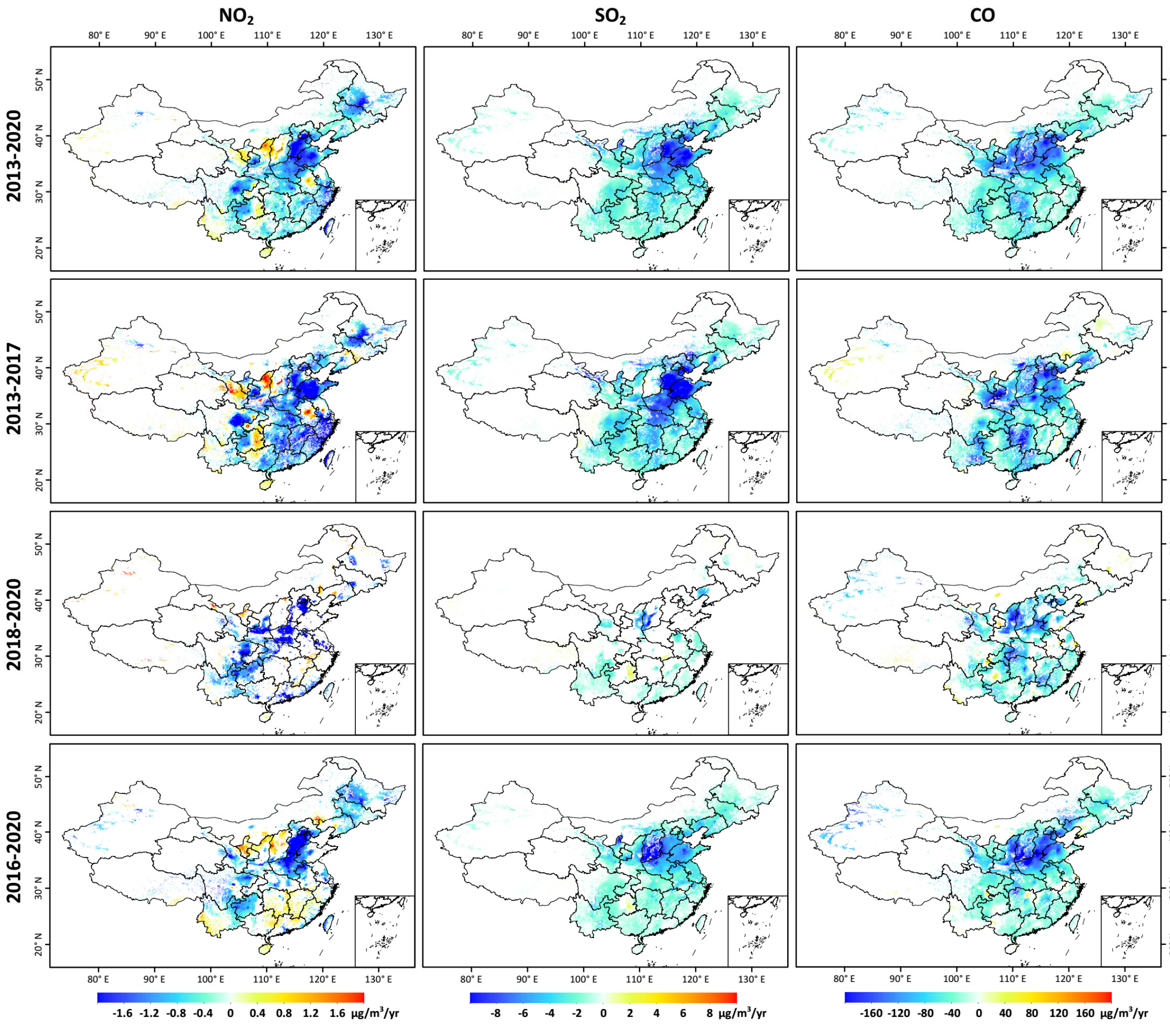

Figure 7. Temporal trends of surface NO_2, SO_2, and CO concentrations during the whole period (2013–2020), the Clean Air Action Plan (2013–2017), the Blue Sky Defense War (2018–2020), and the 13rd Five-Year Plan (2016–2020) in China. Only regions with trends that are significant at the 95% ($p < 0.05$) confidence level are shown.

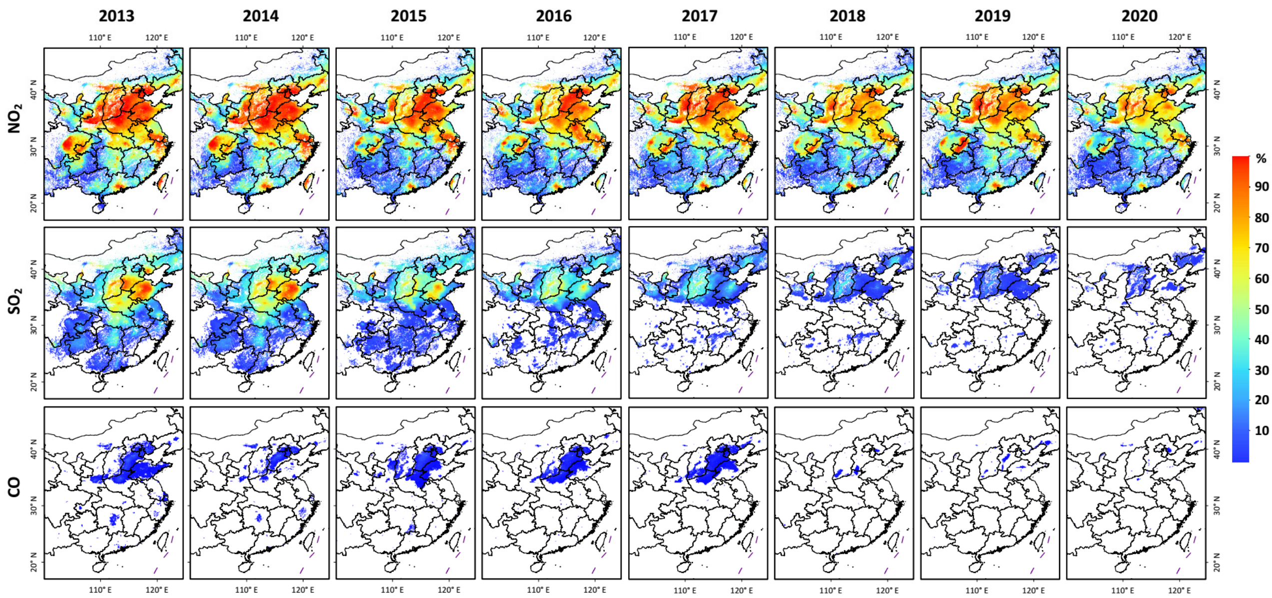

958
959 **Figure 8.** Spatial distributions of the percentage of days exceeding the WHO recommended short-
960 term desired air quality guidelines level for surface NO_2 (daily mean > 25 μg/m^3), SO_2 (daily
961 mean > 40 μg/m^3), and CO (daily mean > 4 mg/m^3) for each year from 2013 to 2020 in populated
962 areas in eastern China.
963

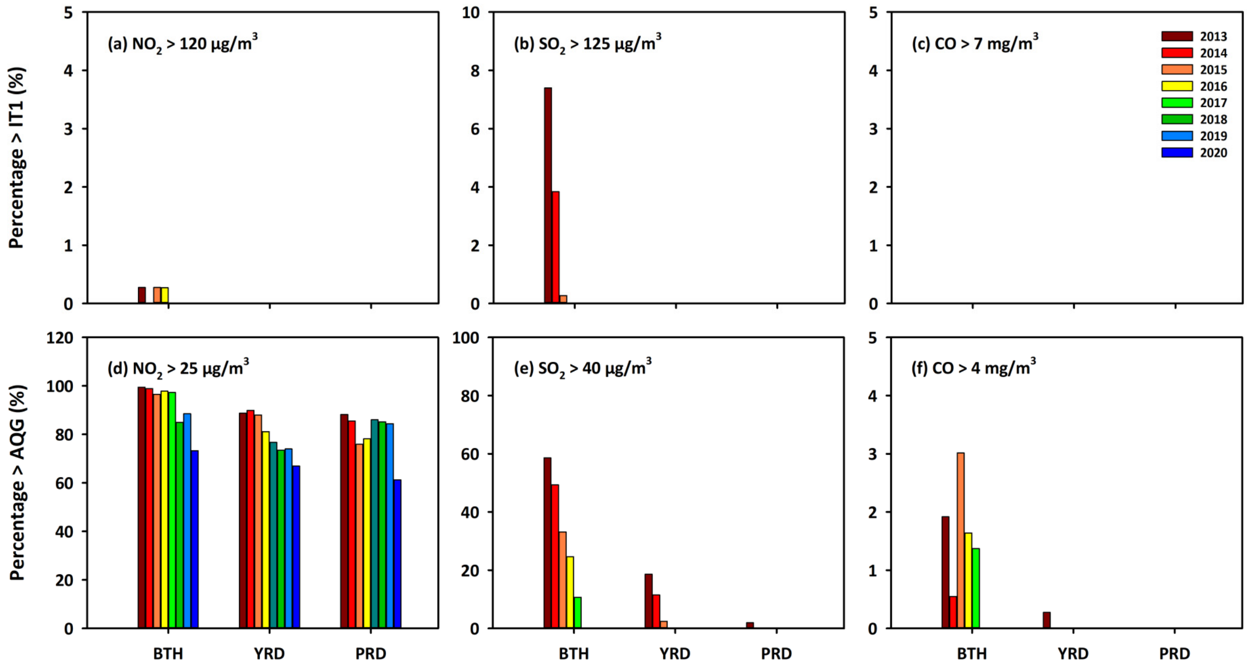

Figure 9. Percentage of days (%) exceeding the WHO recommended short-term (a-c) minimum interim target (IT1) and (d-f) desired air quality guidelines (AQG) level for surface NO_2, SO_2, and CO for each year from 2013 to 2020 in three typical urban agglomerations: the Beijing-Tianjin-Hebei (BTH) region, the Yangtze River Delta (YRD), and the Pearl River Delta (PRD).

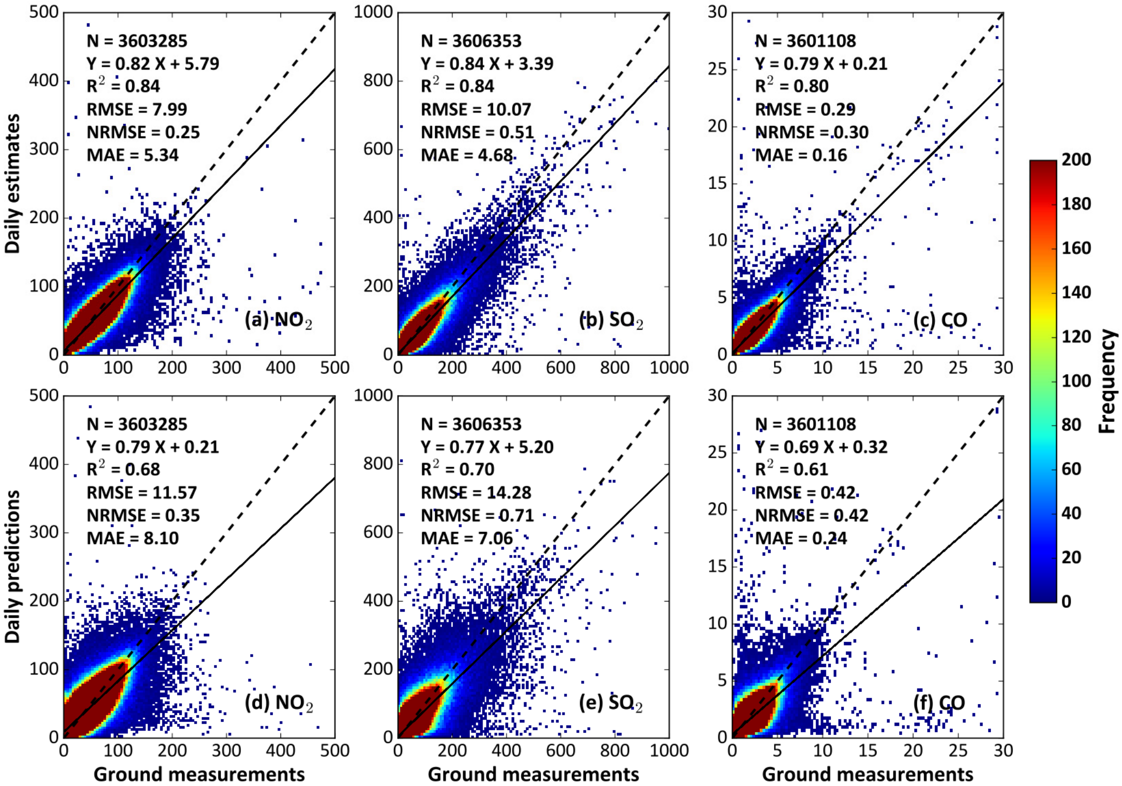

Figure 10. Density plots of daily (a-c) estimates and (d-f) predictions of ground-level NO_2 ($\mu g/m^3$), SO_2 ($\mu g/m^3$), and CO (mg/m^3) concentrations as a function of ground measurements in China from 2013 to 2020 using the out-of-sample (top panels) and out-of-station (bottom panels) cross-validation methods.

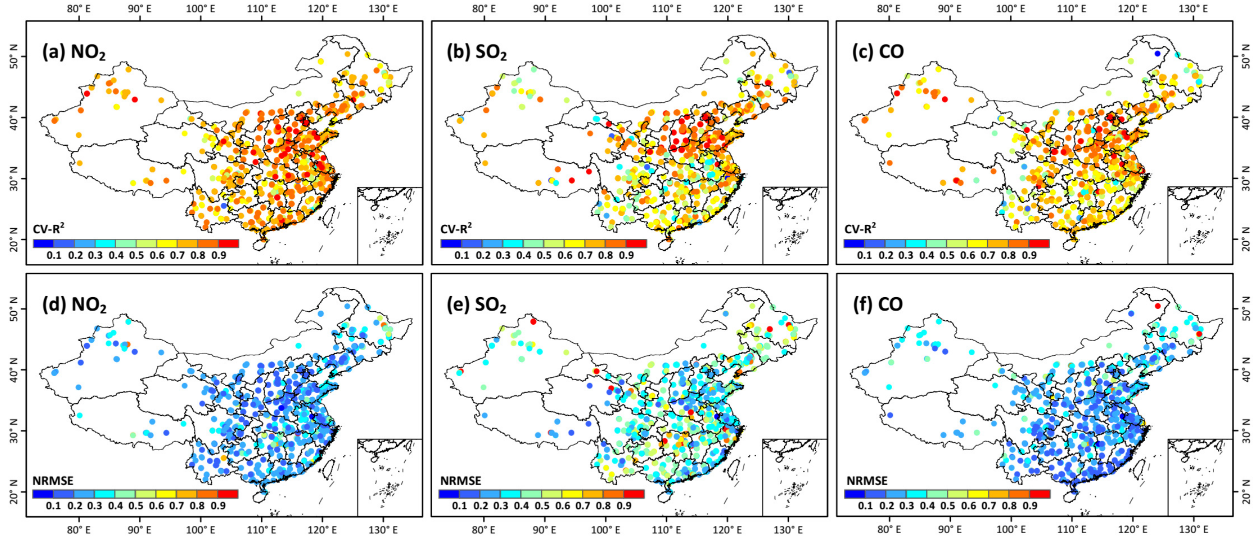

Figure 11. Sample-based spatial validation of daily ground-level NO_2 ($\mu g/m^3$), SO_2 ($\mu g/m^3$), and CO (mg/m^3) estimates at each individual monitoring station in China from 2013 to 2020: (a-c) accuracy (i.e., CV-R^2) and (d-f) uncertainty (i.e., NRMSE).

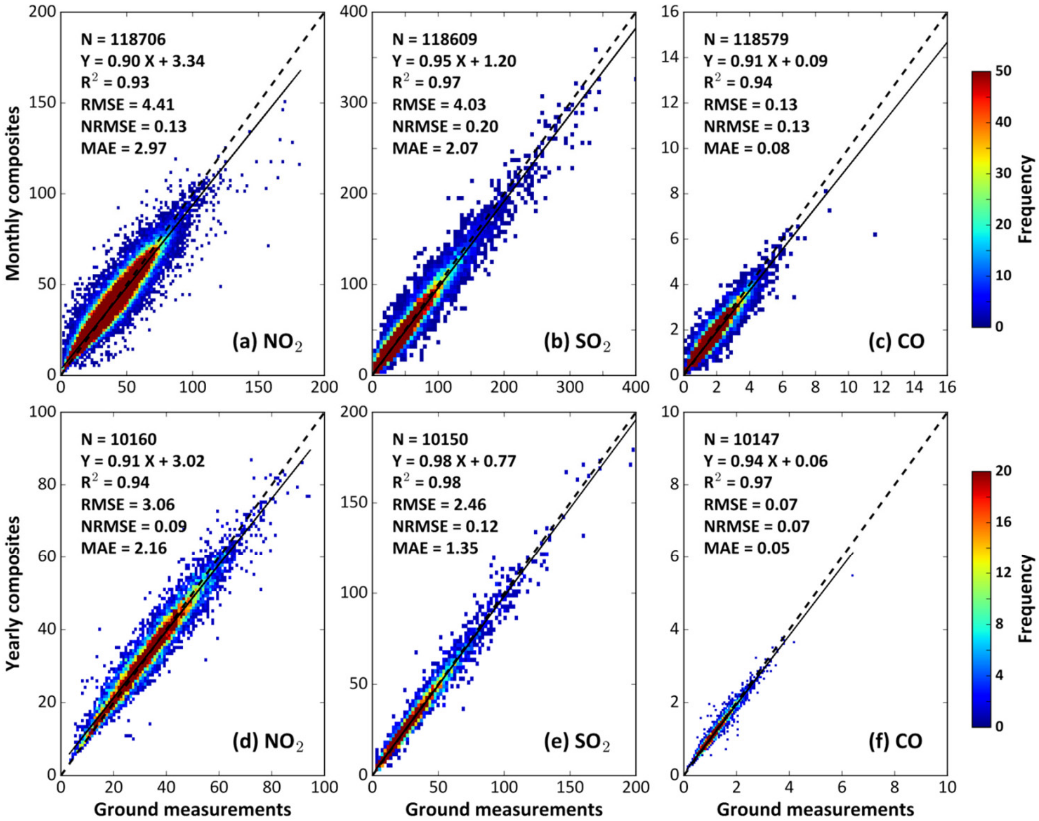

Figure 12. Sample-based temporal validation of (a-c) monthly and (d-f) yearly composites of ground-level NO_2 ($\mu g/m^3$), SO_2 ($\mu g/m^3$), and CO (mg/m^3) as a function of ground measurements from 2013 to 2020 in China.

Tables

Table 1. Statistics of the overall accuracies and predictive abilities of ambient gaseous pollutants for each year in China from 2013 to 2020.

Year	Sample size	Overall accuracy						Predictive ability					
		NO_2		SO_2		CO		NO_2		SO_2		CO	
	N (10^3)	R^2	RMSE	R^2	RMSE	R^2	RMSE	R^2	RMSE	R^2	RMSE	R^2	RMSE
2013	169	0.77	12.48	0.83	17.97	0.80	0.56	0.53	18.16	0.68	25.04	0.60	0.78
2014	324	0.76	10.97	0.83	15.87	0.77	0.38	0.54	15.56	0.66	22.45	0.51	0.57
2015	518	0.79	9.34	0.80	13.71	0.74	0.38	0.61	13.10	0.61	19.49	0.50	0.55
2016	516	0.82	8.59	0.83	11.26	0.76	0.34	0.64	12.20	0.65	16.28	0.57	0.46
2017	527	0.86	7.57	0.86	7.79	0.82	0.24	0.72	10.67	0.74	10.80	0.70	0.32
2018	513	0.87	6.92	0.83	5.61	0.82	0.20	0.76	9.33	0.68	7.80	0.69	0.26
2019	515	0.87	6.78	0.81	4.84	0.82	0.20	0.77	9.23	0.66	6.63	0.70	0.25
2020	522	0.89	5.78	0.80	4.02	0.82	0.17	0.79	8.04	0.62	5.57	0.69	0.23

Table 2. Comparison of long-term datasets of different gaseous pollutants focusing on the whole of China.

Species	Model	Missing values	Spatial resolution	Main input	Validation period	CV-R^2	RMSE	Literature
NO_2	RF-STK	Yes	0.25°	OMI	2013−2016	0.62	13.3	(Zhan et al., 2018)
	RF-K	Yes	0.25°	OMI	2013−2018	0.64	11.4	(Dou et al., 2021)
	KCS	Yes	0.125°	OMI	2014−2016	0.72	7.9	(Z.-Y. Chen et al., 2019)
	LUR	Yes	0.125°	OMI	2014−2015	0.78	-	(H. Xu et al., 2019)
	LME	Yes	0.1°	OMI	2014−2020	0.65	7.9	(Chi et al., 2021)
	XGBoost	Yes	0.125°	TROPOMI	2018−2020	0.67	6.4	(Chi et al., 2022)
	XGBoost	Yes	0.05°	TROPOMI	2018−2019	0.83	7.6	(Liu, 2021)
	LightGBM	No	0.05°	TROPOMI	2018−2020	0.83	6.6	(Y. Wang et al., 2021)
	SWDF	No	0.01°	TROPOMI	2019−2020	0.93	4.9	(Wei et al., 2022b)
	STET	No	0.1°	Big data	2013−2020	0.84	8.0	This study
SO_2	RF	No	0.25°	Emissions	2013−2014	0.64	17.1	(R. Li et al., 2020)
	STET	No	0.1	Big data	2013−2020	0.84	10.1	This study
CO	RF–STK	Yes	0.1	MOPITT	2013−2016	0.51	0.54	(D. Liu et al., 2019)
	LightGBM	No	0.07°	TROPOMI	2018−2020	0.71	0.26	(Y. Wang et al., 2021)
	STET	No	0.1°	Big data	2013−2020	0.80	0.29	This study

KCS: kriging-calibrated satellite method; LightGBM: light gradient boosted model; LME: linear mixed effect model; LUR: land use regression; MOPITT: Measurements of Pollution in the Troposphere; OMI: Ozone Monitoring Instrument; RF: random forest; RF-K: random forest integrated with K-means; RF-STK: random-forest-spatiotemporal-kriging model; STET: space-time extremely randomized tree; SWDF: spatiotemporally weighted deep forest; TROPOMI: TROPOspheric Monitoring Instrument; XGBoost: extreme gradient boosting